

Indolo[3,2-c]quinoline G-Quadruplex Stabilizers: a Structural Analysis of Binding to the Human Telomeric G-Quadruplex

João Lavrado,^{*[a]} Stephan A. Ohnmacht,^[b] Isabel Correia,^[c] Clara Leitão,^[b] Sílvia Pisco,^[b] Mekala Gunaratnam,^[b] Rui Moreira,^[a] Stephen Neidle,^[b] Daniel J. V. A. dos Santos,^[d] and Alexandra Paulo^[a]

A library of 5-methylindolo[3,2-c]quinolones (IQc) with various substitution patterns of alkyldiamine side chains were evaluated for G-quadruplex (G4) binding mode and efficiency. Fluorescence resonance energy transfer melting assays showed that IQcs with a positive charge in the heteroaromatic nucleus and two weakly basic side chains are potent and selective human telomeric (HT) and gene promoter G4 stabilizers. Spectroscopic studies with HT G4 as a model showed that an IQc stabilizing complex involves the binding of two IQc molecules (2,9-bis[3-(diethylamino)propyl]amino-5-methyl-11H-indolo[3,2-c]quinolin-5-ium chloride, **3d**) per G4 unit, in two non-independent but equivalent binding sites. Molecular dynamics studies sug-

gest that end-stacking of **3d** induces a conformational rearrangement in the G4 structure, driving the binding of a second **3d** ligand to a G4 groove. Modeling studies also suggest that **3d**, with two three-carbon side chains, has the appropriate geometry to participate in direct or water-mediated hydrogen bonding to the phosphate backbone and/or G4 loops, assisted by the terminal nitrogen atoms of the side chains. Additionally, antiproliferative studies showed that IQc compounds **2d** (2-[[3-(diethylamino)propyl]amino]-5-methyl-11H-indolo[3,2-c]quinolin-5-ium chloride) and **3d** are 7- to 12-fold more selective for human malignant cell lines than for nonmalignant fibroblasts.

Introduction

Guanine (G)-rich nucleic acid sequences are able to adopt stable four-stranded secondary structures called G-quadruplexes (G4). These DNA structures differ from other nucleic acid structures, as they are composed of stacked coplanar guanine tetrads stabilized by monovalent cations (G-tetrad units), along with connecting loops.^[1] Unlike double-stranded (ds) DNA, G4s can exhibit extensive structural diversity and polymorphism, which depends on various factors:^[2] 1) oligonucleotide strand sequence; 2) strand orientations (e.g. parallel, antiparallel, hybrid); 3) type and size of loops (e.g. diagonal, lateral, double

chain reversal); and 4) solution environment (e.g. Na⁺, K⁺ and dehydration conditions). G4s are highly associated with human diseases such as cancer,^[3] HIV,^[4] and diabetes,^[5] and have been quantitatively visualized in human cells.^[6] Moreover, in the Non-B-DNA Database, over 361 000 putative G4-forming sequences (PQS) have been predicted,^[7] with an enrichment in telomeres, rDNA, promoter regions, untranslated regions of RNA, first exons and introns of many genes.^[8]

In human telomeres (HTs), PQS comprise tandem repeated single-stranded d[AG₃(TTAG₃)₃] sequences, with a 150–200-nucleotide-long single-strand overhang.^[9] This G-overhang acts as a substrate for telomerase, an RNA reverse transcriptase required for telomere extension, which is highly down-regulated in normal cells, resulting in a limit to the number of cell divisions.^[10] However, cancer cells can avoid this natural telomere erosion by means of telomere maintenance mechanisms. Telomerase is overexpressed and up-regulated in ~85% of human cancers, inducing telomere stabilization and cellular immortalization, and its inhibition has been proposed as an effective strategy for the development of new and more selective anti-cancer agents.^[11]

Besides telomeres, G4s have been identified near the transcription starting sites and promoter regions of a number of genes that regulate cell proliferation (e.g. *c-MYC*, *KRAS*, *c-KIT*, *HSP90*, *VEGF*).^[2,12] This appears to suggest a possible function of G4s in controlling gene activity in cells,^[13] and as such may be novel targets for cancer therapy.^[8b,14]

[a] Dr. J. Lavrado, Prof. R. Moreira, Dr. A. Paulo
Research Institute for Medicines (iMed.Ulisboa)
Faculty of Pharmacy, Universidade de Lisboa
Av. Prof. Gama Pinto, 1649-003 Lisbon (Portugal)
E-mail: jplavrado@ff.ulisboa.pt

[b] Dr. S. A. Ohnmacht, C. Leitão, S. Pisco, Dr. M. Gunaratnam, Prof. S. Neidle
The School of Pharmacy, University College London
29/39 Brunswick Square, London WC1N 1AX (UK)

[c] Dr. I. Correia
Centro Química Estrutural
Instituto Superior Técnico, Universidade de Lisboa
Av. Rovisco Pais, 1049-001 Lisboa (Portugal)

[d] Dr. D. J. V. A. dos Santos
REQUIMTE, Department of Chemistry & Biochemistry
Faculty of Sciences, University of Porto
R. do Campo Alegre, 4169-007 Porto

Supporting information for this article is available on the WWW under <http://dx.doi.org/10.1002/cmdc.201500067>.

The particular structure of G4s provides substantial advantages over duplex DNA for small-molecule binding. Therefore, in the last decade an intensive search for small molecules as G4 ligands has led to their development, spanning a wide variety of chemical classes.^[15] According to present knowledge, based mostly on crystallographic, NMR, and molecular modeling studies, the binding mode of these ligands to G4 structures is governed by some simple principles:^[16] 1) Cationic substituents usually result in higher binding affinities. 2) π -Stacking with G-tetrads: large planar aromatic surfaces establish π -stacking interactions with G-tetrads (end-stacking) and importantly, usually have larger surface areas than typical ds DNA ligands, resulting in G4 selectivity. 3) Groove and loop binding: some ligands can bind selectively to the G4 grooves. These ligands can improve selectivity by recognizing a specific groove characteristic in different G4 structures. Notwithstanding, the design of highly efficient G4 ligands remains challenging, in part due to our limited knowledge of the binding modes with many G4s, some of which can be dynamic and polymorphic in structure.

Indolo[3,2-*b*]quinolone (IQb) alkaloids are a well-established class of G4 binders and have emerged with potential applications as antitumor therapeutic agents.^[17] One of the first reports on these compounds was published by Neidle and co-workers, who showed that IQb derivatives stabilize the human telomeric G4, F21T.^[18] Subsequent studies explored IQbs as G4 stabilizers in telomere and oncogene promoter regions and evaluated their bioactivity.^[19] We previously reported the *in vitro* and *in vivo* anticancer profiles of three 5-methyl-IQb derivatives which showed moderate stabilization of the F21T G4.^[20] The study was recently extended to di- and trisubstituted IQb derivatives, and the results suggest that the type, number, and relative position of protonated side chains are important factors that govern binding efficiency and inter-G4 selectivity.^[21]

However, despite numerous G4 binding studies with IQb derivatives, the binding ability of the natural isomer, indolo[3,2-*c*]quinoline (IQc), has not been explored. With this in mind, we decided to evaluate the binding of IQc derivatives (**1**, **2a–g**, and **3c–h**; Figure 1) to several G4 structures and to perform

a comprehensive molecular modeling study on how these IQcs interact with G4s. There is extensive structural knowledge on its polymorphs, and so the human telomeric sequence was used as a general model for G4 binding studies. In broad terms, this will have applicability to future binding studies with other G4 targets, and in particular, will allow the development of IQc derivatives with improved efficiency and selectivity. An IQc G4 binding study was performed using biophysical methods, and insight into DNA flexibility and solvent effects around the binding sites was obtained by molecular modeling. Additionally, to evaluate the effects of IQc compounds in cancer cells, the antiproliferative activity of selected ligands was evaluated in several cell lines.

Results and Discussion

Chemistry

The indolo[3,2-*c*]quinoline (IQc) derivatives **2–3** were prepared from IQc scaffold **1** according to the route depicted in Scheme 1. The synthetic pathway starts with preparation of 4-chloro-6-bromoquinoline (**9**) by Gould–Jacobs cyclization from 4-bromoaniline (**4**).^[22] The synthesis of the IQc nucleus was accomplished by coupling intermediate **9**, as previously described by Molina et al.,^[23] with commercially available 1*H*-benzo[*d*][1,2,3]triazole (**11 a**), or 6-bromo-1*H*-benzo[*d*][1,2,3]triazole (**11 b**) obtained from an ultrasound-assisted reaction of 4-bromobenzene-1,2-diamine (**10**) with sodium nitrite,^[24] to give **12**. Final cyclization, by thermal decomposition of the 1*H*-benzo[*d*][1,2,3]triazole moiety of **12** by means of a Graebe–Ullmann condensation, resulted in the indolo[3,2-*c*]quinolines **1**. Alkylation of IQc **1** was achieved by microwave-assisted reaction with iodomethane followed by treatment with sodium carbonate to give **2a** or **3a–b** in the free-base form. Structures of all compounds were established on the basis of 2D ¹H and ¹³C hetero-correlation NMR experiments (HMQC and HMBC). Assignment of bromine in positions 8 or 9 of the IQc nucleus of **3a** and **3b** was confirmed by NOE difference experiments (Supporting Information).

Synthesis of the final derivatives **2b–g** and **3c–h** was accomplished by microwave-assisted palladium-catalyzed cross-coupling of alkyldiamines with the IQc (**2a**, **3b**, or **3c**) via Buchwald–Hartwig amination. The free-base forms of the IQc derivatives were fully characterized by NMR experiments. The deshielding effect observed for ¹³C NMR signals of C2, C8, and C9 for derivatives **2b–g** and **3c–h** (Supporting Information) confirm the introduction of the alkyldiamine side chains at these positions. The purity of the IQc derivatives **2b–g** and **3c–h** was $\geq 95\%$ as the hydrochlorides (acid form), determined by elemental analysis (Supporting Information).

Thermal stabilization of G4-forming sequences

To evaluate the ability of the IQc derivatives **2–3** to stabilize G4 and ds DNA, initial fluorescence resonance energy transfer (FRET) melting screens were performed with the G4 from the human telomeric sequence (F21T) and with a 26-mer hairpin

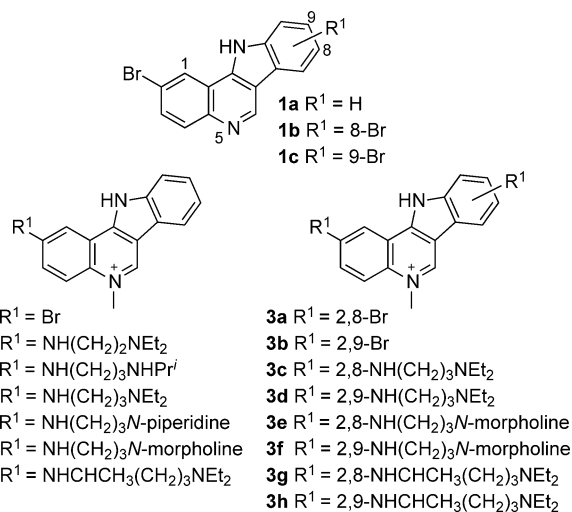
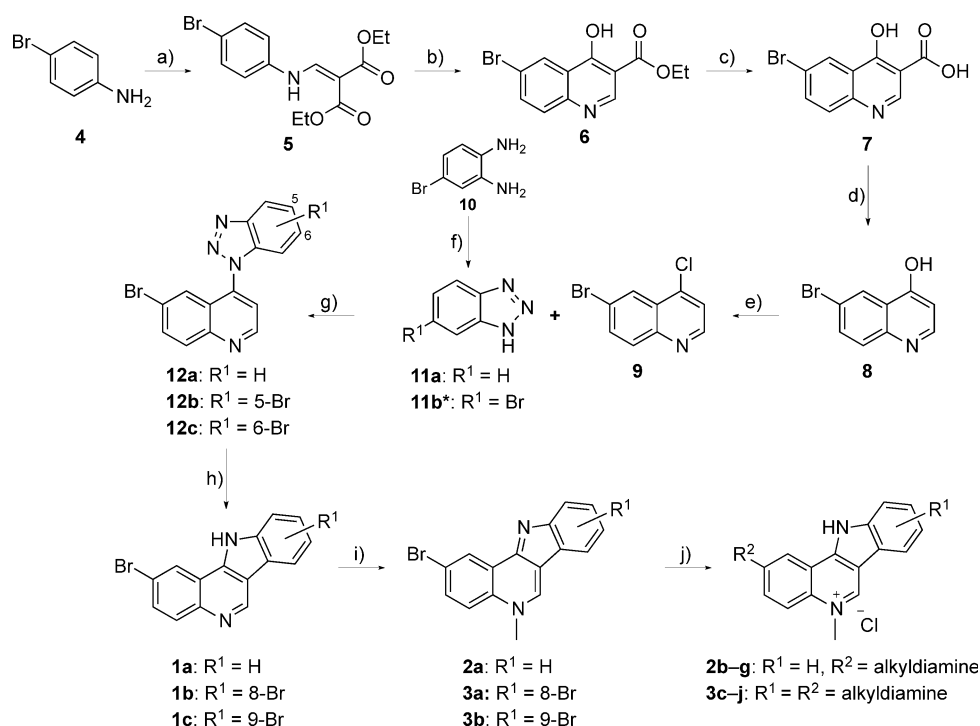


Figure 1. Structures of the indolo[3,2-*c*]quinoline derivatives.



Scheme 1. Synthesis of the indolo[3,2-c]quinoline derivatives. *Reagents and conditions:* a) diethyl-2-(ethoxymethylene)malonate, reflux, 1 h; b) diphenyl ether, reflux, 1 h; c) NaOH (10%), reflux, 1 h; d) diphenyl ether, reflux, 1 h; e) POCl₃, reflux, 2 h; f) NaNO₂, AcOH, sonication (35 KHz), RT, 20 min; g) 120–145 °C, 20 min; h) PPA, 145 °C, 3 h; i) 1. MeI, CH₃CN, 120 °C, 300 W, 2 h, 2. Na₂CO₃ (5%); j) dialkylamine, Pd(OAc)₂, CyJonhPhos, Na₂OBU, DME/tBuOH (1:1), 170 °C, 300 W, 2 h. *Obtained from 10.

loop sequence (T-loop) representing duplex DNA (see Experimental Section below for sequence details). The native F21T G4 and T-loop-tagged sequences (0.2 μM) melt at 61.3 and 53.6 °C, respectively, in potassium cacodylate buffer (pH 7.4, containing 60 mM KCl). The analysis of FRET melting data showed dose-dependent stabilization of F21T G4 and T-loop DNA in the presence of compounds **1**, **2a–g**, and **3c–h** (Figure 2 and Supporting Information). Alkyldiamino-substituted IQc derivatives (1.0 μM) gave Δ*T*_m values ranging from ~12 to 31 °C for F21T G4 and from ~2 to 9 °C for the T-loop, whereas the unsubstituted parent IQc compound **2a** gave values of 5.6 °C (F21T) and 1.5 °C (T-loop), at the same concentration. As described for IQb,^[21,25] alkylation of N5 (**2a**) increases G4 stabilization relative to the non-alkylated IQc **1a**.

In general, 5-methyl-IQc derivatives with one side chain (**2b–g**) show stabilization properties similar to those of mono-substituted 5-methyl-IQb.^[21,26] However, the introduction of a second side chain significantly increases F21T G4 stabilization (**2d** vs. **3c–d**). Substitution pattern is also important for G4 stabilization, as disubstituted IQcs with side chains at positions 2 and 9 (**3d,f,h**) show increased G4 stabilization, compared with their 2,8-disubstituted counterparts (**3c,e,g**).

The wide range of stabilization induced by IQcs in F21T G4 prompted us to evaluate the stabilizing properties of selected IQcs with the G4s from promoter regions of the *HSP90* and *KRAS* oncogenes (Table 1). The results showed similar stabilization of the oncogenic G4, suggesting an equivalent stabiliza-

tion ability of these small molecules to different G4 structures. Moreover, IQc compounds were shown to be as good at G4 stabilization as known G4 ligands with anticancer activity.^[27]

As shown in Figure 2, IQc derivatives stabilize G4s more efficiently than ds DNA, suggesting G4 selectivity. To further assess selectivity of G4s over ds DNA, competitive FRET experiments on F21T G4 (0.2 μM) with **2d** and **3d** were performed in the presence of a non-fluorescent 26-mer ds DNA competitor (26ds). A decrease in Δ*T*_m indicates the displacement of the ligand from G4 by the competitor DNA. The results show that **2d** displacement from F21T by 26ds occurs only at competitor concentrations > 10 μM, showing at least 10-fold G4 selectivity (Supporting Information). On the other hand, displacement of compound **3d** from F21T G4 by 26ds occurred only at competitor concentrations > 25 μM, indi-

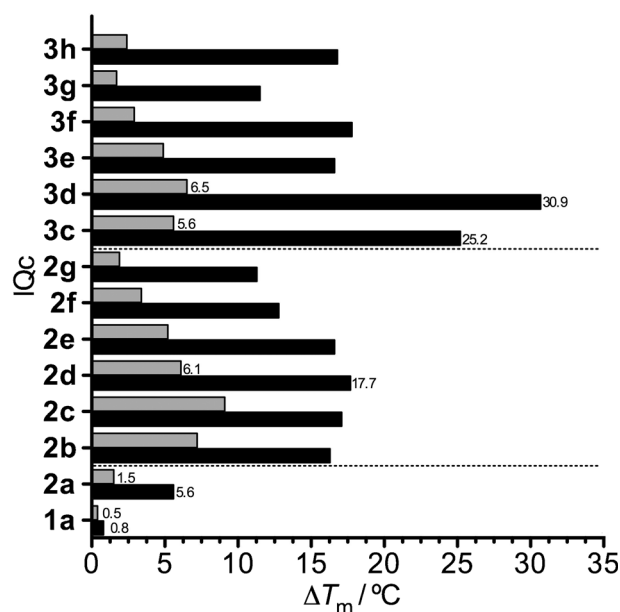


Figure 2. FRET melting temperature variations (Δ*T*_m) of labeled human telomeric G4 (F21T, black bars) and hairpin loop sequence (T-loop, grey bars) at 0.2 μM, stabilized by IQc derivatives **1a**, **2a–g**, and **3c–h** (1 μM) in K⁺ cacodylate buffer (pH 7.4, 60 mM K⁺). Δ*T*_m: SD ≤ 0.2 °C.

cating > 50-fold F21T G4 selectivity over ds DNA (Supporting Information).

IQc	ΔT_m [°C] ^[b]		
	HSP90A ^[c]	KRAS21R ^[d]	KRAS32R ^[e]
1a	0.6	0.7	ND
2a	8.3	4.4	2.2
2d	21.5	15.1	10.7
3d	34.3	22.0	17.0

[a] Determined with promoter regions at 0.2 μM , and IQcs at 1 μM in 60 mM K^+ buffer. [b] $\text{SD} \leq 0.2^\circ\text{C}$. [c] $T_m = 59.0^\circ\text{C}$. [d] $T_m = 52.1^\circ\text{C}$. [e] $T_m = 54.0^\circ\text{C}$.

However, stabilization by the monosubstituted 5-methyl-IQc did not show significant improvement when compared with the values previously reported for the monosubstituted 5-methyl-IQb derivatives;^[26] as such, it seems that both aromatic nuclei (IQb vs. IQc) share similar G4 stabilization properties.

Overall, the FRET screening data revealed that introduction of weakly basic side chains potentiate G4 stabilization and pointed to the 2,9-disubstituted IQc derivative **3d** as the most effective G4 stabilizer among the IQc series evaluated in this study.

Binding affinity for human telomeric G4

Based on the previous FRET screening results, nonsubstituted 5-methyl- (**2a**), mono- (**2d**), and disubstituted-IQc (**3d**) were selected to further characterize IQc G4 binding and probe the effects of the side chains. Due to the large amount of information available on HT G4 structures, such as polymorphism, topology exchange, ligand binding modes and molecular models,^[11d] we choose, for comparison purposes, to use the human telomeric G4 structure as a model system. Spectrofluorimetric titration assays were performed in order to explore the binding behavior of the IQcs to G4 F21T. The emission spectra of compounds **2d** and **3d**, when excited (λ_{ex}) at 290 nm, were characterized by a broad emission band centered at ~ 475 nm, while

for compound **2a** (λ_{ex} 275 nm) the broad emission band showed a maximum peak at ~ 465 nm. Their fluorescence intensities were found to be proportional to concentration up to 10 μM , indicating no significant intermolecular stacking, which would give rise to a quenching effect.

The fluorescence titration spectra of **2a**, **2d**, and **3d** with non-labeled F21T G4 showed fluorescence quenching due to π -stacking interactions (Supporting Information). The fluorescence titration data (Figure 3) were fitted to the Scatchard model (Figure 3, insets).^[28] Scatchard plots are linear for binding to independent and equivalent sites, and any curvature indicates the presence of more than one type of binding, ligand interactions, or neighbor-exclusion effects.^[29]

The titration data for IQc **2a** with F21T G4 showed almost linear fitting to the Scatchard model (Figure 3a, inset), suggesting the presence of either a single site per G4 or an equivalent number of independent binding sites. Further fitting of the fluorescence titration data to the one-site saturation binding equation (Figure 3a) gave an association constant (K_a) of $0.9 \times 10^6 \text{ M}^{-1}$. This behavior is similar to that reported for berberine,^[30] an isoquinoline alkaloid with a single binding mode, having strong π -stacking interactions ($K_a = 1.2 \times 10^6 \text{ M}^{-1}$) with the 22-mer human telomeric G4 d[AG₃(T₂AG₃)₃] (HT22). The present results also suggest a single π -stacking binding mode of **2a** to F21T G4. However, contrary to berberine and some porphyrins, for which external stacking has been ruled out due to splitting and significant increase in emission spectrum intensity,^[30,31] the **2a** fluorescence quenching may indicate external stacking to the G4.

Scatchard plots of **2d** and **3d** (Figure 3b–c, insets) are all concave-down nonlinear curves which may suggest different positive cooperative binding sites, with more than one equivalent and non-independent binding site. The observed quenching of the emission intensity also suggests an external stacking binding mode for **2d** and **3d**. Fitting of the binding data showed no convergence with two-site binding models, possibly due to the similarity between the different types of binding and association constants. Therefore, association constants for **2d** and **3d** were obtained from the one-site saturation binding

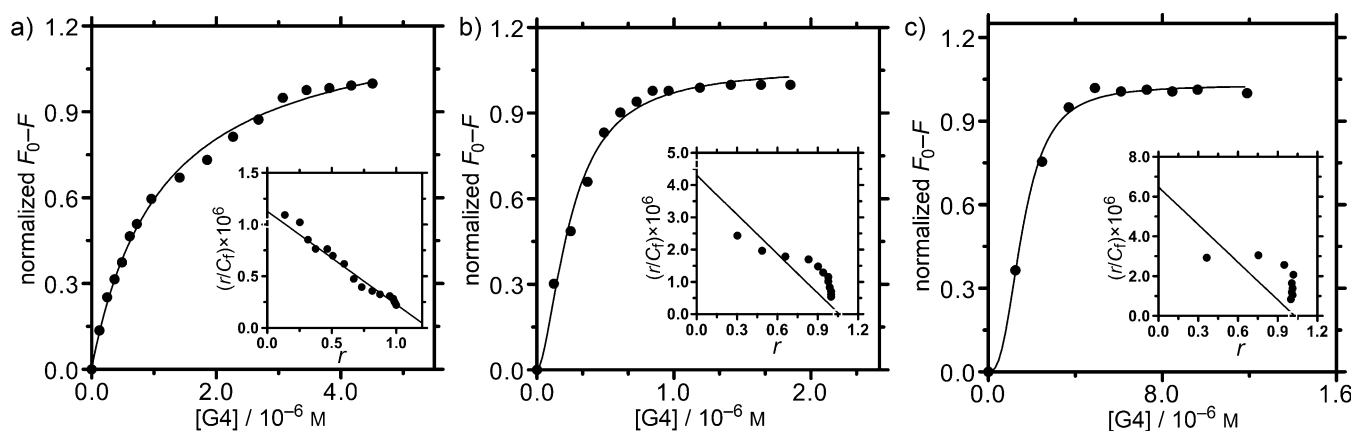


Figure 3. Fluorescence data for a) **2a**, b) **2d**, and c) **3d** at 1 μM , titrated with non-labeled F21T G4 in K^+ cacodylate buffer (pH 7.4, containing 60 mM K^+) at 25 $^\circ\text{C}$, fitted to the saturation binding equations and to the Scatchard model (insets).

with a Hill slope model (Figure 3b–c). These are apparent binding constants, that is, they are macroscopic association constants (K_a) that reflect the total binding without distinction between binding sites. K_a values with HT21 G4 of 4.1 and $6.3 (\times 10^6) \text{ M}^{-1}$ were obtained for **2d** and **3d**, respectively, and Hill constants (h) of 1.7 and 2.7 corroborate the positive cooperativity suggested by the Scatchard analysis. These binding affinities (10^6 M^{-1}) are consistent with those found for other known human telomeric G4 end-stacking ligands, such as zinc porphyrins and acridines ($10^5 \leq K_a \leq 10^7 \text{ M}^{-1}$), as well as with G4 groove binders, such as distamycin.^[32] K_a values for **2a**, **2d**, and **3d** increase with the introduction of alkyldiamine side chains in the heteroaromatic nucleus, which is consistent with the FRET data. From the binding analysis, it also seems that the introduction of side chains induces different IQC binding modes in non-independent sites with positive cooperative effects.

To determine the number of ligand binding sites, continuous variation analysis (Job plot)^[33] of **3d** with F21T was performed (Supporting Information). Plotting of fluorescence as a function of **3d** mole fraction (χ) gave linear dependences at high and low molar fractions, and an intersection of 0.65 was determined (ligand/G4 ratio of 1.85:1). Analogous to IQb end-stacking compounds with HT22 G4 in K^+ solution,^[17a] a stoichiometry of two IQCs per HT G4 unit appears to be favored for the complex equilibrium, complementing results of the saturation binding analysis, which also suggests more than one binding mode. It is feasible that binding of the first ligand may cause a conformational change in the G4 structure, increasing the binding affinity of the second ligand to a different but equivalent binding site.

Structural topology in human telomeric G4

Circular dichroism (CD) spectroscopy was used to examine the topology in the F21T G4 and the effect of ligand binding to further guide molecular modeling studies. The native folding topology of the non-labeled F21T G4 exhibited a CD spectrum typical of a parallel/antiparallel hybrid topology (Supporting Information). This is a positive band having a maximum around 290 nm, a shoulder (+) centered around 270 nm, a weak band (+) with a maximum around 255 nm, and a band (–) with a maximum at 235 nm.^[34]

The titration of HT21 with **3d** caused a gradual suppression of the shoulder at 270 nm, the weak band (+) at 255 nm became a weak band (–) with a maximum at ~260 nm (for a **3d**/HT21 ratio of 10:1), and an isodichroic point arose at 270 nm (Supporting Information). All these observations suggest that the IQC derivative induces a conformational change to an antiparallel G4 topology. According to a recent interpretation of G4 CD spectra reported by da Silva and co-workers,^[35] the set of CD signals induced by **3d** titration appears to point to the formation of a G4 structure containing three stacked tetrads, a diagonal loop, and lateral wide loops. The induced structural transition from hybrid to antiparallel topology also produced very small CD spectral intensity changes around 290 nm which are characteristic of end-stacking ligands, and

are due to ligand-induced changes in the stacking interactions between G4 bases.^[36] Lu et al. reported a structural transition of F21T G4 topology from hybrid to antiparallel induced by 5-methyl-IQb.^[26] Similar results have also been found for other G4 ligands, such as porphyrins, which can induce the transformation from the hybrid-type to an antiparallel G4 in dilute solutions and in the presence of K^+ .^[37]

Molecular dynamics studies

To acquire comprehensive knowledge of IQC–G4 binding modes at an atomistic level, and based on our experimental data, which reveals the binding of two IQCs to the antiparallel HT G4, we performed molecular modeling simulations of **3d** with the antiparallel HT G4, mimicking experimental conditions. This G4 antiparallel structure can exist in the basket- or chair-type forms, and only the former has been determined by NMR solution studies (PDB ID: 143D).^[38] However, on the basis of the CD titration assays, compound **3d** induces the formation of a G4 structure possibly containing three stacked tetrads, a diagonal loop, and lateral wide loops, consistent with the basket-type of 143D. Thus, as a starting model, we used our previously optimized basket-type structure of antiparallel F21T G4.^[21] The structure contains three stacked G-tetrads, which are connected by a central diagonal loop of nucleotides T10, T11, and A12 in the upper G-tetrad and by two lateral loops formed by the bases T4, T5, A6 and by T16, T17, A18 at the other end of the G4 structure (lower G-tetrad). K^+ cations were used to neutralize the system, with two of these ions placed at the center of the G-tetrads. Our spectroscopic studies suggested the binding of two IQC ligands to the F21T G4 unit, with π -stacking interactions, most likely at the G-tetrad ends. Therefore, to evaluate the binding effects on the G4 structure (induced fit) and the influence of the first IQC on the binding of the second IQC (cooperativity), the binding events were simulated sequentially.

Binding of the first ligand

The IQC derivative **3d** was docked with Molecular Operating Environment (MOE)^[39] software, using all of the F21T G4 structure as a potential docking site. The top-ranked positions showed **3d** stacked on the lower G-tetrad, stabilized by π – π stacking and hydrogen bonding with the phosphate backbone (Model 1, Supporting Information).

The lower G-tetrad was more favored than the upper G-tetrad, possibly as a result of the steric hindrance induced by the TTA diagonal loop. Changes in docking protocol, such as different placement algorithms (Alpha Triangle, Alpha PMI and GOLD), scoring functions (Affinity dG and London dG) and restraining the docking site directly to the upper G-tetrad, did not result in the ligand docking on the upper G-tetrad. However, compounds with acridine-based central scaffolds have been described as strong upper G-tetrad binders, with the nucleotides of a diagonal loop stacked above them.^[40] Therefore, **3d** was manually docked with MOE onto the upper G-tetrad and below the diagonal loop, adjusting the ligand position to

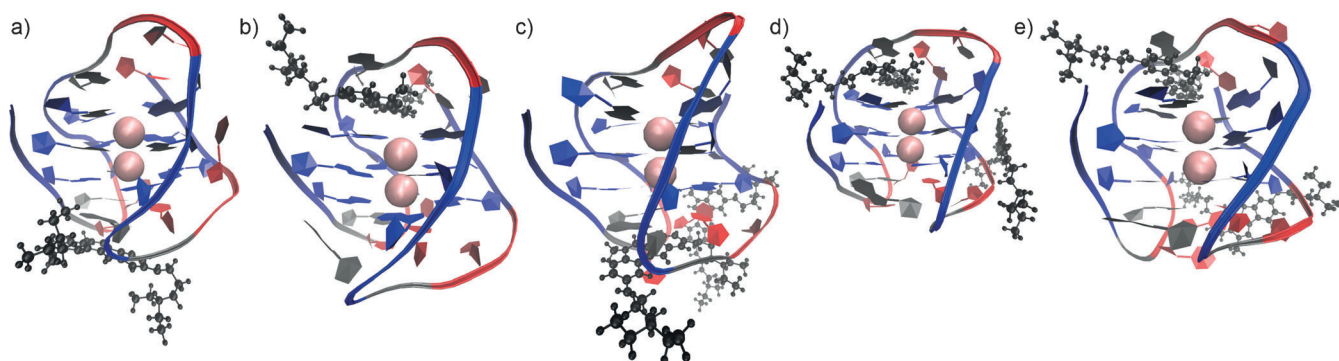


Figure 4. Final MD simulation structures ($t = 50$ ns) of the complexes between one (a and b) and two (c, d, e) indolo[3,2-c]quinoline **3d** with the antiparallel HT21 G4. a) Model 1: lower G-tetrad stacking, b) Model 2: upper G-tetrad stacking, c) Model 1.1: lower G-tetrad stacking and groove binding, d) Model 2.1: upper G-tetrad stacking and groove binding, e) Model 2.2: upper G-tetrad and groove binding. Ligand in CPK representation (black) and G4 structure in ribbons (guanine: blue, thymine: red, adenine: grey, K: pink).

obtain an overall best fit to the G4 structure (Model 2, Supporting Information). Models 1 and 2 were then optimized and equilibrated using multiple minimization steps, followed by 1 ns *NVT* molecular dynamics (MD) run and a final 50 ns isothermal-isobaric ensemble. Final poses are shown in Figure 4a,b.

To assess the overall structural stability of the IQc–G4 complex, we evaluated the root-mean-square deviation (RMSD) of the whole structure, which became stable after 15 ns and carried out trajectory analysis beyond this point. Overall, RMSD values of all ligand atoms in both models (~ 3.0 Å) are similar to RMSD values of the G4 atoms alone, indicating that the IQc ligand is maintained in the binding site of each model. This was also confirmed by visual inspection of the MD run. The aromatic nucleus of **3d** is π -stacked with G-tetrads, while the side chains showed high flexibility, being involved in electrostatic interactions and direct or water-mediated hydrogen bonds with phosphate backbone and/or G4 loops (Supporting Information, Movies 1 and 2).

To explore and quantify the individual contributions to binding affinity, the end-point free energies of interaction in Models 1 and 2 were calculated based on single-trajectory post-processing with the molecular mechanics Poisson–Boltzmann surface area (MM-PBSA) methodology.^[41] This estimates binding free energies that are significantly correlated with experimental data.^[42] The binding free energy and its components in Models 1 and 2 are listed in Table 2. For both models, the binding free energies ($\Delta G_{\text{binding}}$) are negative and closely similar (-56.8 and -58.8 kJ mol⁻¹ for Models 1 and 2, respectively), indicating that both sites are valid binding sites and are in good agreement with values reported elsewhere for G4 complexes.^[43]

The electrostatic energy (ΔE_{elec}) component generally has a larger contribution to complex stabilization than the van der Waals energy (ΔE_{vdw}), especially for Model 2, which has the larger contribution (-13.7 kJ mol⁻¹). The electrostatic contribution is the result of the cationic charges, mainly in the ligand side chains, and is an important factor in IQc binding. This agrees with FRET assay data, in which the increase in IQc side chains from zero to two resulted in a large G4 stabilization.

Table 2. MM-PBSA binding free energies of the antiparallel telomeric G4– 3d complex models studied by MD simulations.					
Free energy ^[a]	1	2	Model 1.1	2.1	2.2
ΔE_{elec}	-12.8	-13.7	-23.1	-20.8	-19.4
ΔE_{vdw}	-6.3	-6.3	-12.4	-12.3	-12.3
$\Delta G_{\text{polar,sol}}$	-1.3	-1.3	-0.2	0.9	1.2
$\Delta G_{\text{nonpolar,sol}}$	-28.8	-28.4	-37.1	-41.7	-43.8
$T\Delta S$	7.6	9.2	9.4	9.2	8.7
$\Delta G_{\text{binding}}$	-56.8	-58.8	-82.2	-83.1	-83.1

[a] Values in kJ mol⁻¹. ΔE_{elec} and ΔE_{vdw} are the molecular mechanics electrostatic and van der Waals contributions, $\Delta G_{\text{polar,sol}}$ and $\Delta G_{\text{nonpolar,sol}}$ are the polar and nonpolar components of the solvation free energy, respectively, $T\Delta S$ is the entropic contribution, and $\Delta G_{\text{binding}}$ is the total binding energy.

ΔE_{vdw} is equal in both models, as the IQc framework provides equivalent vdW contacts. The nonpolar component of the solvation free energy ($\Delta G_{\text{nonpolar,sol}}$) is a highly favorable contribution to complex stabilization in both models, while the electrostatic contribution to the solvation energy ($\Delta G_{\text{polar,sol}}$) is small. Furthermore, the entropic component is also favorable in both models. Ligand binding to the upper G-tetrad (Model 2), over the diagonal loop, represents the most favorable binding mode, with similar geometry to that found experimentally for a series of acridine ligands in a bimolecular G4.^[40]

Binding of the second ligand

A second IQc (**3d**) molecule was docked with MOE software into the final MD simulation structures of Models 1 and 2. The first ten top-ranked docking poses in Model 1 show the second **3d** ligand bound in a G4 groove (T17, A18, G19, G20, and G21; Model 1.1, Supporting Information). Likewise, the binding of a second **3d** in Model 2 also revealed in the first ten top-ranked docking poses, ligand bound in a G4 groove, as well as one **3d** molecule being stacked on the lower G-tetrad. Similar results were recently described by Limongelli and co-workers, for a 3-(benzo[*d*]thiazol-2-yl)-7-hydroxy-2*H*-chromen-2-one G4 ligand in a metadynamics simulation

study.^[44] The ligand followed a hopping binding mode, able to bind both groove and 3' end of the G4. As such, two models were considered, Model 2.1, generated from the first top-ranked docking pose, with **3d** adopting a groove binding conformation in the region of G3, T4, G7, and G8. Model 2.2, generated from the fourth top-ranked pose, has **3d** stacked in the lower G-tetrad in the region of T4, T5, A6, and T17, A18, G19 (Supporting Information).

The final docked complexes were subjected to a 50 ns MD production run simulation, which became stable after the first 10 ns with RMSD values for all G4 atoms of ~ 1.5 Å (Supporting Information). The first **3d** ligand in the lower G-tetrad (Model 1.1) and upper G-tetrad (Models 2.1 and 2.2) was still preserved in the binding site after the binding of the second **3d** molecule (Figure 4c–d and Supporting Information). Similarly, the second **3d** molecules in Models 1.1 and 2.1 were also well retained in their initial binding sites, as shown by RMSD analysis (Figure 4c–d and Supporting Information). However, in Model 2.2, the second **3d** showed, at the end of the MD simulation, an RMSD of ~ 15 Å, revealing displacement of the ligand from the initial binding site in the lower G-tetrad. The analysis of the MD trajectory of Model 2.2 revealed a ligand shift from the lower G-tetrad (Supporting Information, Movie 2.2) to a G4 groove (Figure 4e). Therefore, the MD simulation for Model 2.2 was started with the second **3d** on the lower G-tetrad, while Models 1.1 and 2.1 started with the **3d** in a G4 groove. Thus, all simulated models ended up by anchoring the second ligand in the same G4 groove region (Figure 4c–e). It seems that binding of the first ligand to the upper G-tetrad induced a G4 conformational rearrangement, weakening ligand stacking on the lower G-tetrad, as verified for the first binding event in Model 1. This binding-site dependence is in agreement with the analysis of spectroscopic binding data, which suggests more than one equivalent and non-independent co-operative binding site.

Analysis of the MD trajectory showed, as in Models 1 and 2, consistent π -stacking of the IQc aromatic core with the G4 structure, with the flexible side chains involved in electrostatic interactions and/or hydrogen bonds between G4 groove/loops and water molecules (Supporting Information).

Binding free energies for Models 1.2, 2.1, and 2.2 were obtained by MM-PBSA methodology. ΔE_{elec} and ΔE_{vdw} play important roles in the stabilization of all model complexes, although there is no difference between different binding sites.

The values of $\Delta G_{\text{binding}}$ are very similar, ranging from -83.1 to -82.2 kJ mol⁻¹ (Table 1), indicating that all the proposed binding sites are equally plausible and closely similar to the experimental values obtained for TMPy4 in complex with a HT G4.^[37] Models 2.1 and 2.2 have the lowest $\Delta G_{\text{binding}}$ value (83.1 kJ mol⁻¹). Therefore, matching of binding sites in both models at the end of the MD simulations, in addition to the equivalent free energies of binding, indicates that the upper G-tetrad and a groove are most likely the most favored binding modes of the IQc compound to the antiparallel HT21 G4. Additionally, analysis of the MD runs indicates that disubstituted IQc derivatives with three-carbon side chains possess the appropriate distance between side chain terminal nitrogen

atoms (~ 16 – 18 Å) to fit between G-tetrad deoxyfuranose rings and G4 grooves (17 – 18 Å), corroborating the greater G4 stabilization found in the FRET assays for these derivatives. As shown in Figure 5, **3d** has a length suitable for a connecting bridge

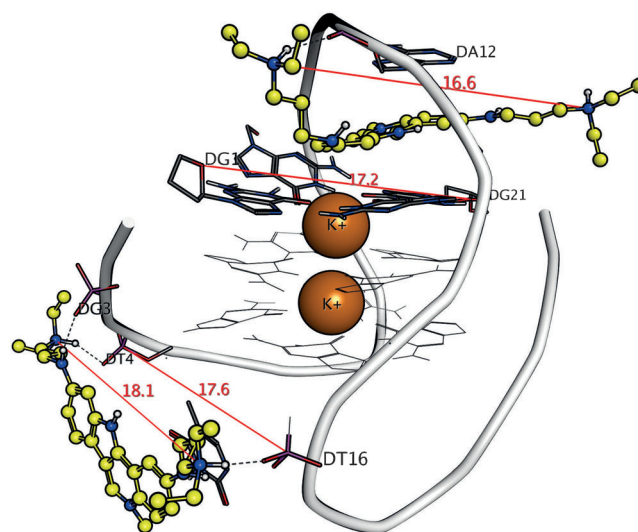


Figure 5. Binding interactions in the **3d**-HT21 G4 complex and lengths (Å) between opposite phosphate backbone and side chains nitrogen atoms of **3d** in Model 2.2. Hydrogen bond: black dashed line; ligand atoms colored by element (carbon: yellow, nitrogen: blue, hydrogen: white); G4 atoms grey or colored by element (carbon: grey, nitrogen: blue, oxygen: red, phosphorus: pink, potassium: orange). Ligands are in ball-and-stick representation, and G4 is in stick and wire representation. Some nucleotides and phosphate backbone have been removed for clarity.

between opposite backbones, stabilized by hydrogen bonds among ligand charged chains and phosphate groups of G4. Overall, these results relate theoretical findings to experimental results, and provide a structural explanation for the G4 stabilization induced by the IQc derivatives.

Antiproliferative activity

The high G4 stabilization and selectivity shown *in vitro* by IQc derivatives prompted us to evaluate their effects on cells. Short-term antiproliferative assays were carried out using a panel of human cancer cell lines and nonmalignant human cell lines, and IC₅₀ values were determined (Table 3).

IQc **2d** and **3d** markedly decreased the viability of cell lines harboring mutated *KRAS*, namely the lung cancer cell line A594, and the pancreatic cancer cell lines (MiaPaCa2, Panc-1), which are both telomerase-positive cell lines. On the other hand, IQcs had a 5–10-fold decreased effect against telomerase-negative cancer lung fibroblasts (ALT).

Derivatives bearing only one side chain (**2d**) showed ~ 3 - to 20-fold lower IC₅₀ values (0.22– 1.93 μM) than IQcs having two basic side chains (**3d**). These differences may be due to variances in cellular uptake by passive diffusion, as compound **2d** would be expected to be more lipophilic than compounds with an additional protonated basic group (**3d**). We also evaluated the selectivity of **2d** and **3d** for cancer cells by assessing

Table 3. Short-term antiproliferative activity for IQCs **2d** and **3d** evaluated with a panel of human malignant and nonmalignant cell lines.

IQc	IC ₅₀ [μ M] ^[a]				
	A594 ^[b]	ALT ^[b]	MiaPaCa2 ^[b]	Panc-1 ^[b]	WI-38 ^[c]
2d	0.40 ± 0.06 (12.5) ^[d]	1.9 ± 0.2	–	0.22 ± 0.07	4.9 ± 0.5
3d	1.45 ± 0.09 (7.0) ^[d]	7.1 ± 0.6	1.9 ± 0.3	4.8 ± 0.2	10.1 ± 0.4

[a] Data are the mean values ±SD of three independent experiments. [b] Malignant cell lines: A594 (lung), ALT (telomerase negative human lung fibroblast), MiaPaCa2 (pancreatic), Panc1 (chemo-resistant pancreatic). [c] Nonmalignant human cell line: WI-38 (lung fibroblast). [d] Selectivity index: IC₅₀(WI-38)/IC₅₀(A594); SD ≤ 0.6.

the effect of these compounds on the viability of a non-cancerous lung fibroblast cell line (WI-38). The results (Table 3) show that these IQc compounds are 12- and 7-fold (**2d** and **3d**, respectively) more selective for the malignant cell line A594 than for nonmalignant fibroblast cells (WI-38).

These results are encouraging, and further studies exploring the mode of action of IQc compounds, via inhibition of telomerase activity and/or repression of *KRAS* expression, are in progress.

Conclusions

G-quadruplex elements in telomeres and in the genome are emerging targets for drug discovery, potentially leading to the development of new drugs with eventually improved selectivity and efficiency over conventional chemotherapeutics. We evaluated a small library of mono- and disubstituted alkyldiamine IQc derivatives, aiming to explore their capacity to induce G4 stabilization and characterize, at a molecular level, their G4 binding interactions using the human telomeric G4 structure (HT21) as a model.

Several derivatives showed very potent thermal stabilization of the HT21 sequence, with ΔT_m values of ~30 °C. Spectroscopic studies revealed that the IQc derivatives **2d** and **3d** stabilize the antiparallel G4 topology of HT21 and form a complex with two ligands per G4 unit. Further analysis of the spectroscopic studies in addition to molecular modeling simulations showed that the disubstituted IQc derivative **3d** binds to the antiparallel human telomeric G4 in two equivalent and non-independent binding sites, in which the second binding event appears to be conditioned by an induced fit to the G4 structure.

Detailed structure analysis and energy calculations show that end stacking of the first ligand in G-tetrad, followed by a second ligand binding to a G4 external groove, are the most favored binding modes. The particular feature of the double substitution pattern with three-carbon side chains (**3d**) allows this ligand to form a bridge between opposite grooves, due to the excellent inter-strand fit of the protonated side chains across the G4 phosphate groups. Such a binding mode will only occur when the geometry of the ligand, and in particular the through-space distance between the protonated nitrogen atoms, is appropriate, as in this case. Thus, as well as π -stack-

ing forces, electrostatic interactions and direct or water-mediated hydrogen bonds, as visualized in ligand-G4 crystal structures,^[45] also play an important role in G4 stabilization.

Selective activity in malignant cell lines relative to nonmalignant human fibroblasts using short-term antiproliferative assays for **2d** and **3d** support the need for further exploration of effects on cancer cells induced by G4 stabilization. The complex interactions detailed in this study, using the human telomeric G4 structure as a model, provide further understanding of binding interactions at an atomic level. These results will aid the design of novel IQc derivatives by exploring G-tetrad and groove binding modes, and open new avenues for the development and optimization of more selective and potent anti-cancer approaches, in tandem with further biological insight into the ultimate cellular targets.

Experimental Section

Chemistry

General: Chemicals were purchased from Sigma–Aldrich Chemical Co. Ltd. (Spain) and were used without further purification. Microwave reactions were performed with a CEM Focused Microwave Synthesis System, Model Discover, equipped with an IntelliVent Pressure Control System. All compounds were characterized by NMR spectroscopy, recorded on a Bruker Avance 400 spectrometer at 400 MHz (¹H NMR) and 100 MHz (¹³C NMR), using solvent as internal reference. Chemical shifts (δ) are expressed in ppm. Signal splitting patterns are described as singlet (s), doublet (d), triplet (t), quartet (q), quintet (quint) and multiplet (m), or a combination thereof. Coupling constants (*J*) are given in Hz. The purity of compounds submitted to biological tests were ≥ 95% in all cases, as determined from elemental C, H, N analysis (Supporting Information), carried out by the Unit for Elemental Analysis, University of Santiago de Compostela (Spain) on a LECO model CHNS-932 elemental analyzer. Mass spectra were recorded using a Micromass Quattro Micro API, Waters. Mass spectra were obtained by direct infusion on “Full Scan” mode (*m/z* 60–800), and sample ionization was made in positive and negative electrospray ionization mode (ESI+ and ESI–). Characterization by high-resolution mass spectrometry (FTIR-MS) was performed in the Faculty of Sciences at the University of Lisbon (Portugal). Melting points (mp) were determined using a Bock-Monoscop M instrument. Reactions were monitored by thin-layer chromatography (TLC) using coated silica gel plates (Merck, aluminum sheets, silica gel 60 F₂₅₄) and aluminum oxide matrix plates (Sigma–Aldrich, PET support, F₂₅₄). Preparative TLC was performed in neutral aluminum oxide 60 G type E (Merck, 200×200 mm glass support). FRET measurements were made on a DNA Engine Opticon (MJ Research), and fluorescence spectroscopy data were collected on a Cary-Eclipse fluorescence spectrophotometer equipped with a Cary Peltier-thermostated cuvette holder with a cell of 1 cm path length. CD spectra were recorded on a JASCO J-720 spectropolarimeter, calibrated with an aqueous solution of 0.06% D-10-(1)-camphor sulfonic acid at 290 nm.

Diethyl-2-[(4-bromophenyl)amino]methylene]malonate (5). A solution of 4-bromoaniline (**4**, 10.0 g, 58.0 mmol) in diethyl 2-(ethoxymethylene)malonate (13.8 g, 12.9 mL, 63.8 mmol, 1.1 equiv) was held at reflux for 1 h. After this period the mixture was cooled to room temperature and added to hexane (300 mL). The precipitate was filtered, washed with hexane and dried to obtain 16.7 g (82%)

of pure **5** as a white solid. $^1\text{H NMR}$ (400 MHz, DMSO): δ = 10.65 (d, J = 9.8 Hz, 1H), 8.35 (d, J = 10.6 Hz, 1H), 7.61–7.47 (m, 2H), 7.36 (d, J = 8.9 Hz, 2H), 4.30–4.07 (m, 4H), 1.24 (t, J = 6.4 Hz, 3H), 1.26 ppm (t, J = 6.4 Hz, 3H).

Ethyl-6-bromo-4-hydroxyquinoline-3-carboxylate (6). A solution of **5** (6.0 g; 17.5 mmol) in diphenyl ether (60 mL) was held at reflux for 1 h. After cooling, the reaction mixture was added to hexane (200 mL) and the formed precipitate was filtered, washed with hexane and dried to obtain 3.18 g (61%) of **6** as a white solid. $^1\text{H NMR}$ (400 MHz, DMSO): δ = 8.59 (s, 1H), 8.23 (d, J = 2.1 Hz, 1H), 7.61 (d, J = 8.2 Hz, 1H), 7.01 (dd, J = 8.2, 2.1 Hz, 1H), 4.23 (q, J = 7.1 Hz, 2H), 1.28 ppm (t, J = 7.1 Hz, 3H).

6-Bromo-4-hydroxyquinoline-3-carboxylic acid (7). A solution of **6** (3.0 g, 10.1 mmol) in NaOH 10% (40 mL) was held at reflux for 1 h. After cooling the reaction mixture to 0–5 °C, the solution was adjusted to pH 1 with HCl (10 M). The formed precipitate was filtered, washed with water and dried to obtain 2.6 g (96%) of **7** as a white solid. $^1\text{H NMR}$ (400 MHz, DMSO): δ = 14.99 (s, 1H), 13.54 (s, 1H), 8.94 (s, 1H), 8.36 (d, J = 2.2 Hz, 1H), 8.04 (dd, J = 8.9, 2.3 Hz, 1H), 7.79 ppm (d, J = 8.9 Hz, 1H).

6-Bromoquinolin-4-ol (8). A solution of **7** (2.5 g, 9.3 mmol) in diphenyl ether (30 mL) was held at reflux for 1 h. The cooled solution was added to hexane (200 mL) and the formed precipitate filtered, washed with hexane and dried to obtain 2.0 g (96%) of **8** as a white solid. $^1\text{H NMR}$ (400 MHz, DMSO): δ = 11.92 (s, 1H), 8.17 (d, J = 2.4 Hz, 1H), 7.95 (d, J = 7.4 Hz, 1H), 7.79 (dd, J = 8.8, 2.4 Hz, 1H), 7.53 (d, J = 8.8 Hz, 1H), 6.08 ppm (d, J = 7.4 Hz, 1H).

6-Bromo-4-chloroquinoline (9). A solution of **8** (2.0 g, 8.9 mmol) in POCl₃ (20 mL) was held at reflux for 2 h. The reaction mixture was cooled, added to water (200 mL) and neutralized with a cold KOH (satd) solution. The formed precipitate was filtered, washed with water and dried to obtain 2.0 g (93%) of **9** as a light-brown solid. $^1\text{H NMR}$ (400 MHz, DMSO): δ = 8.89 (d, J = 4.7 Hz, 1H), 8.35 (d, J = 2.0 Hz, 1H), 8.05 (d, J = 9.0 Hz, 1H), 8.01 (dd, J = 9.0, 2.0 Hz, 1H), 7.84 ppm (d, J = 4.7 Hz, 1H); $^{13}\text{C NMR}$ (100 MHz, DMSO): δ = 151.6, 147.6, 140.6, 134.4, 132.3, 127.3, 126.1, 123.0, 122.0 ppm.

6-Bromo-1H-benzo[d][1,2,3]triazole (11 b). A solution of 4-bromo-1,2-diaminobenzene (**10**, 2.0 g, 10.7 mmol) and sodium nitrite (1.84 g, 26.7 mmol, 2.5 equiv) in AcOH (20 mL) was sonicated at 35 KHz for 20 min at room temperature. After this period the reaction mixture was added to water (250 mL) and extracted with EtOAc (3 × 200 mL). The combined organic extracts were washed with water (200 mL), dried with brine and anhydrous Na₂SO₄. After solvent removal under reduced pressure, the crude product was purified by recrystallization from boiling EtOH with water to obtain 2.0 g (95%) of **11 b** as a light-brown solid; mp: 133–135 °C. $^1\text{H NMR}$ (400 MHz, DMSO): δ = 15.99 (s broad, NH), 8.29 (s, 1H), 7.99 (d, J = 8.8 Hz, 1H), 7.66 (dd, J = 8.8, 1.6 Hz, 1H); $^{13}\text{C NMR}$ (100 MHz, DMSO) 143.8, 142.1, 130.0, 128.9, 117.9, 117.3 ppm; MS (ESI+) C₆H₄BrN₃ calcd [M+H]⁺ 199.96, found [M+H]⁺ 200.08.

General Procedure A. 4-(1H-Benzo[d][1,2,3]triazol-1-yl)-6-bromoquinoline (12 a). Homogenized 6-bromo-4-chloroquinoline **9** (1.0 g, 4.1 mmol) and benzotriazole (**11 a**, 0.491 g, 4.1 mmol) were heated at 120 °C for 20 min. The resulting solid was cooled to room temperature and subsequently recrystallized from boiling EtOH with water, to give **12 a** as a white solid (1.27 g, 95%). $^1\text{H NMR}$ (400 MHz, DMSO): δ = 9.23 (d, J = 4.6 Hz, 1H), 8.31 (d, J = 8.4 Hz, 1H), 8.22 (d, J = 9.0 Hz, 1H), 8.08 (dd, J = 9.0, 2.2 Hz, 1H), 8.01 (dd, J = 5.5, 3.4 Hz, 2H), 7.78 (d, J = 8.3 Hz, 1H), 7.71 (ddd, J = 7.9, 5.9, 0.9 Hz, 1H), 7.61 ppm (ddd, J = 8.0, 6.8, 1.0 Hz, 1H); $^{13}\text{C NMR}$

(100 MHz, DMSO): δ = 152.3, 148.4, 145.8, 139.1, 134.4, 133.8, 132.3, 129.8, 125.8, 125.8, 124.1, 122.1, 120.4, 118.8, 111.4 ppm.

6-Bromo-4-(5-bromo-1H-benzo[d][1,2,3]triazol-1-yl)quinoline (12 b) and 6-bromo-4-(6-bromo-1H-benzo[d][1,2,3]triazol-1-yl)quinoline (12 c). A mixture of **9** (2.5 g, 10.3 mmol) and **11 b** (2.04 g, 10.3 mmol) was reacted at 145 °C according to General Procedure A. The crude product was purified via flash column chromatography on silica gel using hexane/EtOAc (8:2) as eluent, to obtain **12 b** (1.44 g, 35%) as a light-brown solid and **12 c** (2.20 g, 52%) as a white solid. **12 b**: $^1\text{H NMR}$ (400 MHz, CDCl₃): δ = 9.17 (d, J = 4.6 Hz, 1H), 8.43 (d, J = 1.2 Hz, 1H), 8.18 (d, J = 9.0 Hz, 1H), 8.00 (d, J = 2.0 Hz, 1H), 7.95 (dd, J = 9.0, 2.1 Hz, 1H), 7.72 (dd, J = 8.8, 1.7 Hz, 1H), 7.62 (d, J = 4.6 Hz, 1H), 7.40 ppm (d, J = 8.8 Hz, 1H); $^{13}\text{C NMR}$ (100 MHz, CDCl₃): δ = 150.63, 148.71, 147.28, 139.15, 134.56, 132.64, 132.55, 131.86, 125.38, 123.94, 123.33, 122.97, 118.35, 117.53, 111.21 ppm. **12 c**: $^1\text{H NMR}$ (400 MHz, CDCl₃): δ = 9.17 (d, J = 4.6 Hz, 1H), 8.18 (d, J = 9.0 Hz, 1H), 8.13 (d, J = 8.7 Hz, 1H), 8.03 (d, J = 2.1 Hz, 1H), 7.95 (dd, J = 9.0, 2.1 Hz, 1H), 7.71 (d, J = 1.1 Hz, 1H), 7.65 (dd, J = 8.7, 1.6 Hz, 1H), 7.61 ppm (d, J = 4.6 Hz, 1H); $^{13}\text{C NMR}$ (100 MHz, CDCl₃): δ = 150.6, 148.8, 144.9, 139.1, 134.6, 134.6, 131.8, 128.9, 125.4, 124.1, 123.8, 123.0, 121.8, 117.4, 112.9 ppm.

General Procedure B. 2-Bromo-11H-indolo[3,2-c]quinoline (1 a). A mixture of **12 a** (1.27 g, 3.9 mmol) in PPA (40.0 g) was heated at 140–150 °C until the release of N₂ ceased. After 3 h the reaction mixture was added to cold water (200 mL), neutralized with KOH (satd) and the precipitate collected by filtration, washed with water and dried under reduced pressure, to give **1 a** as a light-yellow solid (1.10 g, 95%). $^1\text{H NMR}$ (400 MHz, DMSO): δ = 12.82 (s, 1H), 9.64 (s, 1H), 8.81 (d, J = 2.2 Hz, 1H), 8.34 (d, J = 7.8 Hz, 1H), 8.08 (d, J = 8.9 Hz, 1H), 7.86 (dd, J = 8.9, 2.2 Hz, 1H), 7.74 (d, J = 8.2 Hz, 1H), 7.52 (dd, J = 8.2, 7.6 Hz, 1H), 7.34 ppm (dd, J = 7.8, 7.6 Hz, 1H); $^{13}\text{C NMR}$ (100 MHz, DMSO): δ = 145.9, 144.4, 139.3, 139.1, 132.2, 131.3, 126.4, 124.9, 122.1, 121.3, 120.8, 118.9, 118.8, 115.3, 112.5 ppm.

2,8-Dibromo-11H-indolo[3,2-c]quinoline (1 b). A mixture of **12 b** (1.0 g, 2.5 mmol) and PPA (30 g) was reacted according to General Procedure B to give **1 b** as a light-brown solid (0.335 g, 36%). $^1\text{H NMR}$ (400 MHz, DMSO): δ = 12.91 (s, 1H), 9.64 (s, 1H), 8.76 (s, 1H), 8.59 (s, 1H), 8.06 (d, J = 8.8 Hz, 1H), 7.86 (d, J = 8.8 Hz, 1H), 7.68 (d, J = 8.3 Hz, 1H), 7.62 ppm (d, J = 8.3 Hz, 1H); $^{13}\text{C NMR}$ (100 MHz, DMSO): δ = 146.2, 144.7, 139.8, 138.0, 132.3, 131.7, 128.9, 125.0, 124.0, 123.5, 119.1, 118.8, 114.5, 114.4, 113.6 ppm.

2,9-Dibromo-11H-indolo[3,2-c]quinoline (1 c). A mixture of **12 c** (1.0 g, 2.5 mmol) and PPA (40 g) was reacted according to General Procedure B to give **1 c** as a light-brown solid (0.487 g, 52%). $^1\text{H NMR}$ (400 MHz, DMSO): δ = 13.00 (s, 1H), 9.62 (s, 1H), 8.80 (d, J = 2.2 Hz, 1H), 8.28 (d, J = 8.4 Hz, 1H), 8.06 (d, J = 8.9 Hz, 1H), 7.90 (d, J = 1.5 Hz, 1H), 7.86 (dd, J = 8.9, 2.2 Hz, 1H), 7.49 ppm (dd, J = 8.4, 1.5 Hz, 1H); $^{13}\text{C NMR}$ (100 MHz, DMSO): δ = 145.9, 144.5, 140.1, 139.5, 132.2, 131.6, 125.0, 124.2, 122.54, 121.2, 119.1, 119.0, 118.8, 115.1, 114.9 ppm.

General Procedure C. 2-Bromo-5-methyl-5H-indolo[3,2-c]quinoline (2 a). A mixture of **1 a** (0.5 g, 1.7 mmol) and Mel (2.39 g, 1.04 mL, 17.0 mmol) in CH₃CN (5 mL) was stirred, in a closed vessel, under microwave radiation (P_{max} = 300 W) at 120 °C for 2 h. After this period, the solvent was removed at reduced pressure. The remaining residue was suspended in Na₂CO₃ 5% aqueous solution (100 mL) and extracted with CH₂Cl₂ (3 × 50 mL). Combined organic extracts were dried with brine and anhydrous Na₂SO₄, and the solvent removed under reduced pressure to give **2 a** as a dark-yellow solid (0.382 g, 76%). $^1\text{H NMR}$ (400 MHz, CDCl₃): δ = 8.80 (d, J =

2.3 Hz, 1H), 7.95 (d, $J=8.6$ Hz, 1H), 7.78 (s, 1H), 7.77 (d, $J=8.9$ Hz, 1H), 7.58 (d, $J=8.6$ Hz, 1H), 7.54 (dd, $J=8.8$, 2.3 Hz, 1H), 7.31 (dd, $J=8.9$, 7.5 Hz, 1H), 7.27 (dd, $J=8.8$, 7.5 Hz, 1H), 3.82 ppm (s, 3H); ^{13}C NMR (100 MHz, CDCl_3): $\delta=154.5$, 152.1, 135.2, 133.7, 131.9, 126.8, 126.6, 125.1, 121.9, 120.8, 119.3, 119.0, 118.8, 117.6, 117.3, 42.4 ppm.

General Procedure D. 2-[[2-(Diethylamino)ethyl]amino]-5-methyl-11H-indolo[3,2-c]quinolin-5-ium chloride (2b). A solution of **2a** (50.0 mg, 0.16 mmol), 2-(dicyclohexylphosphino)biphenyl (CyJohnPhos, 11.2 mg, 0.032 mmol), $\text{Pd}(\text{OAc})_2$ (7.2 mg, 0.032 mmol), NaOtBu (61.5 mg, 0.64 mmol) and N^1,N^1 -diethylethane-1,2-diamine (74.4 mg, 89.9 μL , 0.64 mmol) in $t\text{BuOH}/\text{DME}$ (1:1, 2 mL) was stirred in a closed vessel, under microwave radiation ($P_{\text{max}}=300$ W) at 170 °C for 2 h. After cooling to room temperature, the crude mixture was filtered over Celite 545, the solid washed with $\text{CH}_2\text{Cl}_2/\text{MeOH}$ (9:1) and the filtrate evaporated under reduced pressure. The residue was then suspended in Na_2CO_3 5% aqueous solution (50 mL) and extracted with CH_2Cl_2 (3 \times 50 mL). The combined organic extracts were dried with brine, anhydrous Na_2SO_4 and concentrated under reduced pressure. Purification by preparative TLC on neutral aluminum oxide, using $\text{CH}_2\text{Cl}_2/\text{MeOH}$ (9:1) as eluent and desorbent from the aluminum oxide, gave **2b** as a dark-yellow solid (29.3 mg, 56%). After NMR characterization, **2b** was precipitated in its salt form, from CH_2Cl_2 (2 mL) with HCl in Et_2O , filtered and dried under reduced pressure. ^1H NMR (400 MHz, CDCl_3): $\delta=7.99$ (s, 1H), 7.89 (d, $J=8.0$ Hz, 1H), 7.74 (s, 1H), 7.73 (d, $J=8.2$ Hz, 1H), 7.42 (dd, $J=8.0$, 7.5 Hz, 1H), 7.22 (d, $J=8.8$ Hz, 1H), 7.17 (dd, $J=8.2$, 7.5 Hz, 1H), 6.86 (d, $J=8.8$ Hz, 1H), 3.82 (s, 3H), 3.28–3.20 (m, 2H), 2.73 (t, $J=5.0$ Hz, 2H), 2.59 (q, $J=7.0$ Hz, 4H), 1.06 ppm (t, $J=7.0$ Hz, 6H); ^{13}C NMR (100 MHz, CDCl_3): $\delta=147.1$, 134.6, 130.2, 128.6, 126.4, 125.2, 122.6, 120.7, 119.6, 119.3, 118.2, 117.9, 115.6, 103.1, 51.9, 47.2, 43.4, 41.7, 12.4 ppm.

2-[[3-(Isopropylamino)propyl]amino]-5-methyl-11H-indolo[3,2-c]quinolin-5-ium chloride (2c). Reaction of **2a** (50.0 mg, 0.16 mmol), CyJohnPhos (11.2 mg, 0.032 mmol), $\text{Pd}(\text{OAc})_2$ (7.2 mg, 0.032 mmol), NaOtBu (61.5 mg, 0.64 mmol) and N^1 -isopropylpropane-1,3-diamine (74.4 mg, 89.6 μL , 0.64 mmol) in $t\text{BuOH}/\text{DME}$ (1:1, 2 mL), followed by purification according to General Procedure D gave **2c** as a dark-yellow solid (23.0 mg, 41%). ^1H NMR (400 MHz, CDCl_3): $\delta=7.95$ (s, 1H), 7.93 (d, $J=7.5$ Hz, 1H), 7.76 (d, $J=7.7$ Hz, 1H), 7.72 (s, 1H), 7.45 (dd, $J=7.7$, 7.5 Hz, 1H), 7.21 (d, $J=8.1$ Hz, 1H), 7.19 (dd, $J=7.7$, 7.2 Hz, 1H), 6.83 (d, $J=8.1$ Hz, 1H), 3.80 (s, 3H), 3.30 (t, $J=6.6$ Hz, 2H), 2.83 (dd, $J=12.5$, 6.2 Hz, 1H), 2.77 (t, $J=6.5$ Hz, 2H), 1.86 (m, 2H), 1.10 ppm (t, $J=6.2$ Hz, 6H); ^{13}C NMR (100 MHz, CDCl_3): $\delta=152.2$, 151.7, 146.4, 133.7, 127.9, 125.7, 124.9, 122.4, 119.9, 118.9, 118.4, 118.0, 117.2, 115.3, 102.1, 48.9, 45.8, 43.1, 42.5, 29.5, 22.9 ppm.

2-[[3-(Diethylamino)propyl]amino]-5-methyl-11H-indolo[3,2-c]quinolin-5-ium chloride (2d). A solution of **2a** (50.0 mg, 0.16 mmol), CyJohnPhos (11.2 mg, 0.032 mmol), $\text{Pd}(\text{OAc})_2$ (7.2 mg, 0.032 mmol), NaOtBu (61.5 mg, 0.64 mmol) and N^1,N^1 -diethylpropane-1,3-diamine (83.3 mg, 100.9 μL , 0.64 mmol) in $t\text{BuOH}/\text{DME}$ (1:1, 2 mL) was reacted and purified according to General Procedure D to give **2d** as a dark-yellow solid (16.2 mg, 28%). ^1H NMR (400 MHz, CDCl_3): $\delta=8.02$ (s, 1H), 7.94 (d, $J=7.6$ Hz, 1H), 7.78 (s, 1H), 7.77 (d, $J=7.4$, 1H), 7.45 (dd, $J=7.6$, 7.4 Hz, 1H), 7.26 (d, $J=9.1$ Hz, 1H), 7.20 (dd, $J=7.4$, 7.1 Hz, 1H), 6.85 (d, $J=9.1$ Hz, 1H), 3.83 (s, 3H), 3.32 (t, $J=6.0$ Hz, 2H), 2.64–2.54 (m, 6H), 1.85 (q, $J=6.7$ Hz, 2H), 1.08 ppm (t, $J=7.1$ Hz, 6H); ^{13}C NMR (100 MHz, CDCl_3): $\delta=152.4$, 151.7, 146.7, 133.8, 127.9, 125.7, 125.0, 122.5, 119.9, 118.9, 118.3, 118.0, 117.2, 115.3, 102.2, 52.2, 46.9, 43.9, 42.6, 25.9, 11.8 ppm; FTIR-MS: predicted: 361.24, found: 361.23829.

5-Methyl-2-[[3-(piperidin-1-yl)propyl]amino]-11H-indolo[3,2-c]quinolin-5-ium chloride (2e). A solution of **2a** (50.0 mg, 0.16 mmol), CyJohnPhos (11.2 mg, 0.032 mmol), $\text{Pd}(\text{OAc})_2$ (7.2 mg, 0.032 mmol), NaOtBu (61.5 mg, 0.64 mmol) and 3-(piperidin-1-yl)propan-1-amine (91.4 mg, 102.1 μL , 0.64 mmol) in $t\text{BuOH}/\text{DME}$ (1:1, 2 mL) was reacted and purified according to General Procedure D to give **2e** as a dark-yellow solid (28.8 mg, 48%). ^1H NMR (400 MHz, CDCl_3): $\delta=8.31$ (s, 1H), 7.77 (d, $J=9.1$ Hz, 1H), 7.75 (d, $J=8.3$ Hz, 1H), 7.53 (s, 1H), 7.37 (dd, $J=9.1$, 7.6 Hz, 1H), 7.29 (d, $J=8.5$ Hz, 1H), 7.16 (dd, $J=8.3$, 7.6 Hz, 1H), 6.82 (d, $J=8.5$ Hz, 1H), 4.03 (s, 3H), 3.26 (m, 2H), 2.50 (t, $J=6.4$ Hz, 2H), 2.50–2.42 (m, 4H), 1.92–1.80 (t, $J=6.0$ Hz, 2H), 1.70–1.62 (m, 4H), 1.57–1.45 ppm (m, 2H); ^{13}C NMR (100 MHz, CDCl_3): $\delta=147.3$, 134.8, 127.8, 126.4, 123.3, 120.9, 120.5, 119.6, 119.3, 117.6, 115.9, 114.1, 101.1, 58.2, 54.8, 43.6, 43.3, 26.4, 25.4, 24.6 ppm.

5-Methyl-2-[[3-(morpholinopropyl)amino]-11H-indolo[3,2-c]quinolin-5-ium chloride (2f). Reaction of **2a** (50.0 mg, 0.16 mmol), CyJohnPhos (11.2 mg, 0.032 mmol), $\text{Pd}(\text{OAc})_2$ (7.2 mg, 0.032 mmol), NaOtBu (61.5 mg, 0.64 mmol) and 3-morpholinopropan-1-amine (92.2 mg, 93.5 μL , 0.64 mmol) in $t\text{BuOH}/\text{DME}$ (1:1, 2 mL), followed by purification according to General Procedure D gave **2f** as a dark-yellow solid (29.5 mg, 49%). ^1H NMR (400 MHz, CDCl_3): $\delta=7.97$ (s, 1H), 7.96 (d, $J=7.7$ Hz, 1H), 7.80 (d, $J=1.9$ Hz, 1H), 7.78 (d, $J=8.1$ Hz, 1H), 7.47 (dd, $J=7.7$, 7.6 Hz, 1H), 7.26 (d, $J=8.7$ Hz, 1H), 7.23 (dd, $J=8.1$, 7.6 Hz, 1H), 6.87 (dd, $J=8.7$, 1.9 Hz, 1H), 3.81 (s, 3H), 3.84–3.68 (m, 4H), 3.33 (t, $J=6.0$ Hz, 2H), 2.52 (t, $J=6.5$ Hz, 2H), 2.55–2.45 (m, 4H), 1.86 ppm (2t, $J=6.5$, 6.0 Hz 2H); ^{13}C NMR (100 MHz, CDCl_3): $\delta=154.1$, 153.0, 146.9, 134.2, 128.7, 126.2, 125.9, 123.4, 120.5, 119.5, 119.0, 118.9, 117.8, 116.2, 102.9, 67.7, 58.2, 54.5, 44.1, 43.1, 26.0 ppm.

2-[[5-(Diethylamino)pentan-2-yl]amino]-5-methyl-11H-indolo[3,2-c]quinolin-5-ium chloride (2g). A solution of **2a** (50.0 mg, 0.16 mmol), CyJohnPhos (11.2 mg, 0.032 mmol), $\text{Pd}(\text{OAc})_2$ (7.2 mg, 0.032 mmol), NaOtBu (61.5 mg, 0.64 mmol) and N^1,N^1 -diethylpentane-1,4-diamine (101.3 mg, 124.0 μL , 0.64 mmol) in $t\text{BuOH}/\text{DME}$ (1:1, 2 mL) was reacted and purified according to General Procedure D to give **2g** as a dark-yellow solid (30.1 mg, 48%). ^1H NMR (400 MHz, CDCl_3): $\delta=8.15$ (s, 1H), 7.91 (d, $J=7.9$ Hz, 1H), 7.86 (s, 1H), 7.79 (d, $J=7.6$ Hz, 1H), 7.42 (dd, $J=7.9$, 7.4 Hz, 1H), 7.30 (d, $J=9.2$ Hz, 1H), 7.18 (dd, $J=7.6$, 7.4 Hz, 1H), 6.86 (d, $J=9.2$ Hz, 1H), 3.90 (s, 3H), 3.72 (m, Hz, 1H), 2.53 (q, $J=7.1$ Hz, 4H), 2.42 (t, $J=6.5$ Hz, 2H), 1.66–1.52 (m, 4H), 1.25 (d, $J=6.8$ Hz, 3H), 1.02 ppm (t, $J=7.1$ Hz, 6H); ^{13}C NMR (100 MHz, CDCl_3): $\delta=152.0$, 151.0, 145.8, 134.1, 127.9, 125.8, 124.9, 122.4, 120.1, 119.1, 118.4, 117.8, 117.5, 115.3, 103.0, 52.8, 48.5, 46.7, 42.6, 35.0, 23.7, 20.6, 11.5 ppm.

5-Methyl-2,8-dibromo-5H-indolo[3,2-c]quinoline (3a). Reaction of **1b** (0.5 g, 1.3 mmol) and Mel (1.88 g, 0.828 mL, 13.0 mmol) in CH_3CN (5 mL) according to General Procedure C, gave **3a** as a dark-yellow solid (0.332 g, 62%). ^1H NMR (400 MHz, DMSO): $\delta=9.53$ (s, 1H), 8.86 (d, $J=2.2$ Hz, 1H), 8.34 (d, $J=2.0$ Hz, 1H), 8.08 (d, $J=9.2$ Hz, 1H), 8.03 (dd, $J=9.2$, 2.2 Hz, 1H), 7.74 (d, $J=8.6$ Hz, 1H), 7.58 (dd, $J=8.6$, 2.0 Hz, 1H), 4.28 ppm (s, 3H); ^{13}C NMR (100 MHz, DMSO): $\delta=152.2$, 150.6, 140.9, 134.9, 132.9, 128.9, 127.4, 126.4, 122.9, 122.3, 121.0, 120.1, 119.3, 115.8, 113.2, 43.4 ppm.

5-Methyl-2,9-dibromo-5H-indolo[3,2-c]quinoline (3b). Reaction of **1c** (0.5 g, 1.3 mmol) and Mel (1.88 g, 0.828 mL, 13.0 mmol) in CH_3CN (5 mL) according to General Procedure C, gave **3b** as a dark-orange solid (0.352 g, 68%). ^1H NMR (400 MHz, DMSO): $\delta=9.39$ (s, 1H), 8.81 (s, 1H), 8.05 (d, $J=8.3$ Hz, 1H), 8.01 (d, $J=9.0$ Hz, 1H), 7.98 (d, $J=9.0$ Hz, 1H), 7.95 (s, 1H), 7.39 (d, $J=8.3$ Hz, 1H), 4.23 ppm (s, 3H); ^{13}C NMR (100 MHz, DMSO): $\delta=156.2$, 152.8,

139.7, 134.8, 132.5, 126.2, 125.0, 123.1, 122.9, 121.7, 121.5, 120.7, 118.9, 118.7, 116.5, 42.9 ppm.

2,8-Bis[3-(diethylamino)propylamino]-5-methyl-11H-indolo[3,2-c]quinolin-5-ium chloride (3c). A solution of **3a** (50.0 mg, 0.13 mmol), CyJohnPhos (9.1 mg, 0.026 mmol), Pd(OAc)₂ (5.8 mg, 0.026 mmol), NaOtBu (99.9 mg, 1.04 mmol) and *N*¹,*N*¹-diethylpropane-1,3-diamine (135.4 mg, 163.8 μL, 1.04 mmol) in *t*BuOH/DME (1:1, 2 mL) was reacted and purified according to General Procedure D to give **3c** as a dark-orange solid (12.3 mg, 20%). ¹H NMR (400 MHz, CDCl₃): δ = 8.23 (s, 1H), 7.76 (s, 1H), 7.55 (d, *J* = 7.0 Hz, 1H), 7.36 (d, *J* = 8.6 Hz, 1H), 7.02 (s, 1H), 6.86 (d, *J* = 8.6 Hz, 1H), 6.50 (d, *J* = 8.0 Hz, 1H), 4.09 (s, 3H), 3.40–3.32 (m, 2H), 3.28 (t, *J* = 6.2 Hz, 2H), 2.64–2.54 (m, 12H), 1.85 (m, 4H), 1.11–1.06 ppm (m, 12H); ¹³C NMR (100 MHz, CDCl₃): δ = 152.2, 151.9, 149.3, 147.5, 133.8, 128.4, 125.6, 122.5, 120.4, 120.1, 117.9, 115.6, 110.4, 102.0, 99.2, 53.0, 52.8, 47.6, 47.5, 44.7, 44.6, 43.9, 26.9, 26.5, 12.6, 12.6 ppm.

2,9-Bis[3-(diethylamino)propylamino]-5-methyl-11H-indolo[3,2-c]quinolin-5-ium chloride (3d). A solution of **3b** (50.0 mg, 0.13 mmol), CyJohnPhos (9.1 mg, 0.026 mmol), Pd(OAc)₂ (5.8 mg, 0.026 mmol), NaOtBu (99.9 mg, 1.04 mmol) and *N*¹,*N*¹-diethylpropane-1,3-diamine (135.4 mg, 163.8 μL, 1.04 mmol) in *t*BuOH/DME (1:1, 2 mL) was reacted and purified according to General Procedure D to give **3d** as a dark-orange solid (15.8 mg, 25%). ¹H NMR (400 MHz, CDCl₃): δ = 7.94 (s, 1H), 7.64 (s, 1H), 7.45 (d, *J* = 8.0 Hz, 1H), 7.22 (d, *J* = 8.2 Hz, 1H), 7.00 (s, 1H), 6.79 (d, *J* = 8.2 Hz, 1H), 6.50 (d, *J* = 8.0 Hz, 1H), 4.04 (s, 3H), 3.42–3.37 (m, 2H), 3.39–3.35 (m, 2H), 2.74–2.65 (m, 12H), 2.05–1.94 (m, 4H), 1.28–1.20 ppm (m, 12H); ¹³C NMR (100 MHz, CDCl₃): δ = 152.9, 151.5, 149.2, 147.2, 133.1, 128.3, 124.1, 121.3, 120.3, 119.5, 117.8, 115.9, 110.2, 102.2, 97.6, 52.9, 52.8, 47.6, 47.5, 44.7, 44.4, 43.7, 26.9, 26.6, 12.6, 12.5 ppm; FTIR-MS: predicted: 489.37, found: 490.36928.

5-Methyl-2,8-bis[3-(morpholinopropyl)amino]-11H-indolo[3,2-c]quinolin-5-ium chloride (3e). A solution of **3a** (50.0 mg, 0.13 mmol), CyJohnPhos (9.1 mg, 0.026 mmol), Pd(OAc)₂ (5.8 mg, 0.026 mmol), NaOtBu (99.9 mg, 1.04 mmol) and 3-morpholinopropan-1-amine (149.9 mg, 151.9 μL, 1.04 mmol) in *t*BuOH/DME (1:1, 2 mL) was reacted and purified according to General Procedure D to give **3e** as a dark-orange solid (17.3 mg, 25%). ¹H NMR (400 MHz, CDCl₃): δ = 8.40 (s, 1H), 7.86 (s, 1H), 7.77 (d, *J* = 7.8 Hz, 1H), 7.48 (d, *J* = 8.6 Hz, 1H), 7.17 (s, 1H), 7.03 (d, *J* = 8.6 Hz, 1H), 6.91 (dd, *J* = 7.3 Hz, 1H), 4.16 (s, 3H), 3.99–8.86 (m, 8H), 3.44–3.36 (m, 4H), 2.76–2.64 (m, 12H), 2.06–2.00 ppm (m, 4H); ¹³C NMR (100 MHz, CDCl₃): δ = 151.7, 151.3, 148.9, 146.7, 132.6, 128.7, 121.8, 120.2, 119.4, 117.7, 115.5, 110.0, 101.9, 101.6, 67.9, 67.7, 58.4, 58.2, 54.5, 54.5, 44.4, 44.1, 43.2, 26.3, 26.0 ppm.

5-Methyl-2,9-bis[3-(morpholinopropyl)amino]-11H-indolo[3,2-c]quinolin-5-ium chloride (3f). A solution of **3b** (50.0 mg, 0.13 mmol), CyJohnPhos (9.1 mg, 0.026 mmol), Pd(OAc)₂ (5.8 mg, 0.026 mmol), NaOtBu (99.9 mg, 1.04 mmol) and 3-morpholinopropan-1-amine (149.9 mg, 151.9 μL, 1.04 mmol) in *t*BuOH/DME (1:1, 2 mL) was reacted and purified according to General Procedure D to give **3f** as a dark-orange solid (29.8 mg, 45%). ¹H NMR (400 MHz, CDCl₃): δ = 8.10 (s, 1H), 7.78 (s, 1H), 7.56 (d, *J* = 8.2 Hz, 1H), 7.35 (d, *J* = 9.0 Hz, 1H), 7.07 (s, 1H), 6.87 (d, *J* = 9.0 Hz, 1H), 6.55 (d, *J* = 8.2 Hz, 1H), 4.04 (s, 3H), 3.80–3.68 (m, 8H), 3.38–3.26 (m, 4H), 2.61–2.39 (m, 12H), 1.90–1.84 ppm (m, 4H); ¹³C NMR (100 MHz, CDCl₃): δ = 153.9, 150.5, 148.2, 146.3, 133.9, 128.0, 125.2, 122.0, 121.8, 119.6, 118.5, 117.0, 114.8, 109.2, 102.1, 101.2, 67.1, 67.1, 57.7, 57.5, 53.8, 53.8, 43.3, 43.3, 42.5, 25.5, 25.3 ppm.

2,8-Bis[5-(diethylamino)pentan-2-ylamino]-5-methyl-11H-indolo[3,2-c]quinolin-5-ium chloride (3g). A solution of **3a** (50.0 mg, 0.13 mmol), CyJohnPhos (9.1 mg, 0.026 mmol), Pd(OAc)₂ (5.8 mg, 0.026 mmol), NaOtBu (99.9 mg, 1.04 mmol) and *N*¹,*N*¹-diethylpentane-1,4-diamine (164.6 mg, 201.4 μL, 1.04 mmol) in *t*BuOH/DME (1:1, 2 mL) was reacted and purified according to General Procedure D to give **3g** as a dark-orange solid (11.2 mg, 16%). ¹H NMR (400 MHz, CDCl₃): δ = 8.09 (s, 1H), 7.84 (s, 1H), 7.58 (d, *J* = 8.0 Hz, 1H), 7.37 (d, *J* = 8.7 Hz, 1H), 7.09 (s, 1H), 6.90 (d, *J* = 8.7 Hz, 1H), 6.53 (d, *J* = 7.7 Hz, 1H), 4.13 (s, 3H), 3.91–3.81 (m, 1H), 3.73 (d, *J* = 4.8 Hz, 1H), 2.71–2.61 (m, 8H), 2.64–2.52 (m, 4H), 1.75 (s, 8H), 1.43 (d, *J* = 4.8 Hz, 6H), 1.26–1.14 ppm (m, 12H); ¹³C NMR (100 MHz, CDCl₃): δ = 152.6, 151.9, 147.9, 146.5, 132.9, 128.5, 124.0, 122.1, 120.3, 119.4, 117.9, 115.3, 110.4, 103.5, 100.0, 53.7, 49.5, 49.2, 47.5, 47.4, 43.5, 35.8, 35.8, 24.4, 24.4, 21.5, 21.4, 12.3, 12.3 ppm.

2,9-Bis[5-(diethylamino)pentan-2-ylamino]-5-methyl-11H-indolo[3,2-c]quinolin-5-ium chloride (3h). A solution of **3b** (50.0 mg, 0.13 mmol), CyJohnPhos (9.1 mg, 0.026 mmol), Pd(OAc)₂ (5.8 mg, 0.026 mmol), NaOtBu (99.9 mg, 1.04 mmol) and *N*¹,*N*¹-diethylpentane-1,4-diamine (164.4 mg, 201.4 μL, 1.04 mmol) in *t*BuOH/DME (1:1, 2 mL) was reacted and purified according to General Procedure D to give **3h** as a dark-orange solid (15.8 mg, 22%). ¹H NMR (400 MHz, CDCl₃): δ = 8.00 (s, 1H), 7.84 (s, 1H), 7.53 (d, *J* = 7.8 Hz, 1H), 7.34 (d, *J* = 8.6 Hz, 1H), 7.11 (s, 1H), 6.86 (d, *J* = 8.6 Hz, 1H), 6.52 (d, *J* = 7.8 Hz, 1H), 4.12 (s, 3H), 3.93–3.80 (m, 1H), 3.78–3.72 (m, 1H), 2.67 (dq, *J* = 6.9, 6.7 Hz, 8H), 2.61–2.53 (m, 4H), 1.81–1.71 (m, 8H), 1.44 (d, *J* = 6.6, 6H), 1.26–1.14 ppm (m, 12H); ¹³C NMR (100 MHz, CDCl₃): δ = 153.1, 152.1, 148.2, 147.3, 133.2, 128.2, 124.3, 121.9, 120.0, 118.5, 116.2, 115.3, 114.0, 109.9, 103.5, 102.6, 99.4, 53.7, 53.6, 50.1, 49.1, 47.4, 47.4, 44.1, 35.8, 35.6, 24.5, 24.4, 21.6, 21.4, 12.3, 12.1 ppm.

Oligonucleotides: All oligonucleotides were purchased from Eurofins MWG Synthesis GmbH (Germany) or StabVida Genomics Lab, Caparica, Lisbon (Portugal). Labeled oligonucleotides used in the FRET assays had attached the donor fluorophore FAM (6-carboxyfluorescein) and the acceptor fluorophore TAMRA (6-carboxytetramethylrhodamine): F21T (5'-[FAM]-GGGT TAGG GTAG GGTT AGGG-[TAMRA]-3'), T-loop (5'-[FAM]-TATA GCTA TATT TTTT TATA GCTA TA-[TAMRA]-3'), HSP90A (5'-[FAM]-GGGC CAAA GGGA AGGG GTGG G-[TAMRA]-3'), KRAS21R (5'-[FAM]-AGGG CCGT GTGG GAAAG AGGG A-[TAMRA]-3'), KRAS32R (5'-[FAM]-AGGG CCGT GTGG GAAAG AGGG AAGA GGGG GAGG-[TAMRA]-3'). A non-fluorescent 26-mer double-stranded oligonucleotide (ds26: 5'-CAAT CGGA TCGA ATTC GATC CGAT TG-3') was used in the competition assays. The non-labeled oligonucleotide from the human telomeric sequence (F21T: 5'-GGGT TAGG GTAG GGTT AGGG-3') was used in the spectroscopic studies. Each oligonucleotide was initially diluted to a storage solution at 100 μM in nuclease-free water (not DEPC-treated), purchased from Ambion Applied Biosystems (UK).

Biological methods

FRET melting assays: The ability of indolo[3,2-c]quinolines to stabilize DNA sequences was investigated using a fluorescence resonance energy transfer (FRET) assay as reported elsewhere.^[21]

Fluorescence spectroscopy binding studies: Fluorescence data were collected with λ_{ex} 290 nm and λ_{em} ~475 nm for the indolo[3,2-c]quinolines **2d** and **3d**, and λ_{ex} 275 nm and λ_{em} ~460 nm for **2a**. Test compounds were prepared as 1 mM stock solutions in HPLC-grade water (10% DMSO). The rest of the dilutions were performed using K⁺ cacodylate buffer (pH 7.4, containing 60 mM K⁺). The G4 oligonucleotide single-stranded sequences were initially diluted

from the storage solution (100 μM) with K^+ cacodylate buffer pH 7.4, containing 60 mM K^+ (10 mM K^+ cacodylate, 50 mM KCl) to a stock solution at 25 μM . The titration data were obtained by adding aliquots of previously annealed G4 stock solutions (heating at 95 $^\circ\text{C}$ for 10 min, followed by slow cooling to RT) to a solution of the indolo[3,2-*c*]quinoline ligand (1 μM) in K^+ cacodylate buffer pH 7.4, 60 mM K^+ , at 25 $^\circ\text{C}$. The titration data were used to construct Scatchard plots with the concentration of bound and free ligand (C_b and C_f , respectively) calculated from the fluorescence values [Eq. (1)] and [Eq. (2)].

$$C_b = (F_f - F) / (F_f - F_b) C \quad (1)$$

$$C_f = C - C_b \quad (2)$$

F_f is the fluorescence of the free ligand, F_b is the fluorescence of the bound ligand, F is the fluorescence of a mixture of free and bound ligand at any point during titration, and C is the total concentration of ligand. From these data, the values of r , the number of moles of ligand bound to 1 mol of G4 ($r = C_b / C_{\text{DNA}}$) were calculated. Saturation binding isotherms were represented as Scatchard plots, by plotting r/C_f vs. r and evaluated according to the model of McGhee and von Hippel. Dissociation constants were determined by fitting the titration experimental data to the one-site saturation binding equation [Eq. (3)] or to the one-site saturation binding to the Hill slope equation [Eq. (4)] supplied with the GraphPad Prism software package, ver. 5.00 (GraphPad Software, San Diego, CA, USA), on the basis of the primary analysis made by Scatchard plots.

$$y = (x F_{\text{max}} / K_d + x) \quad (3)$$

$$y = (x F_{\text{max}} / K_d^h + x^h) \quad (4)$$

F_{max} is the saturated binding fluorescence extrapolated to very high concentrations of G4, and h is the Hill constant. If h equals 1.0, the ligand binds with no cooperativity to one site. If $h > 1$ the receptor or ligand has multiple binding sites with positive cooperativity, and if $h < 1$ there are multiple binding sites with different affinities for ligand or when there is negative cooperativity. Association constants (K_a) were calculated from dissociation constants (K_d). Lines represented in the Scatchard plots were calculated from the data fitting to the binding equations ($x=0$, $y = F_{\text{max}}/K_d$; $x = F_{\text{max}}$, $y = 0$; slope = $-K_a$).

Binding stoichiometry: The binding stoichiometry of IQc derivative **3d** with G4 was obtained by spectrofluorimetry using the Job method of continuous variation at 25 $^\circ\text{C}$.^[33] Test compound was prepared as 1 mM stock solutions in HPLC-grade water (10% DMSO). Dilution to working solution (25 μM) was performed using K^+ cacodylate buffer (pH 7.4, containing 60 mM K^+). Previously annealed stock solutions (heating at 95 $^\circ\text{C}$ for 10 min, followed by slow cooling to RT) at 25 μM of the non-labeled oligonucleotide sequences F21T in K^+ cacodylate buffer (pH 7.4, 60 mM K^+) were as working solution. Total concentration of ligand and G4 in the solutions was kept constant ($[\mathbf{3d}] + [\text{G4}] = 4 \mu\text{M}$). Changes in fluorescence intensity were monitored as a function of the mole fraction (χ) of the indolo[3,2-*c*]quinoline derivative. The intercept of the two best-fit lines obtained by least-squares linear regression analysis, obtained with GraphPad Prism ver. 5.00, indicated the binding stoichiometry of the complex. Fluorescence data were normalized according to F normalized = $(F_{\text{max}} - F) / (F_{\text{max}} - F_{\text{min}})$, for which F is fluorescence, F_{max} is maximum value of F , and F_{min} is the minimum value of F .

CD measurements: CD spectra were recorded with a JASCO 720 spectropolarimeter, with a photomultiplier suitable for the 200–700 nm range. Unless otherwise stated, CD spectra provide a representation of molar ellipticity values ($[\theta]$ in $\text{deg cm}^2 \text{dmol}^{-1}$) vs. λ ($[\theta] = 3298.2 \times \Delta\epsilon$; $\Delta\epsilon = \text{differential absorption} / (bC)$, where $b = \text{optical path}$ and $C = \text{total DNA concentration}$). All measurements and operations of the spectropolarimeter were computer controlled. Test compounds were prepared as 1 mM stock solutions in HPLC-grade water (10% DMSO). The rest of the dilutions were performed using K^+ cacodylate buffer (pH 7.4, containing 60 mM K^+). The CD spectra shown are the average of three scans, recorded at 25 $^\circ\text{C}$, of previously annealed (heating at 95 $^\circ\text{C}$ for 10 min, followed by slow cooling to RT) 5 μM non-labeled human telomeric sequence F21T in K^+ cacodylate buffer. CD spectra of titrations with indolo[3,2-*c*]quinoline **3d** (added aliquots of 500 μM stock solution in K^+ cacodylate buffer pH 7.4, 60 mM K^+) were collected between 220 and 320 nm using 10 mm path-length cuvettes. Buffer baseline was subtracted from each spectrum. The following parameters were used for data collection: data pitch 0.5 nm, band width 1 nm, response 2 s, and scan speed 100 nm min^{-1} .

Sulforhodamine B (SRB) short-term cytotoxicity assay: Human cell lines, breast carcinoma (MCF7), lung carcinoma (A549), pancreatic cancer (MiaPaCa2, Panc-1), immortalized telomerase-negative human lung fibroblast (ALT) and normal human lung fibroblast (WI-38), were all purchased from American Type Culture Collection (ATCC). Cell lines were maintained in appropriate medium supplemented with 10% fetal bovine serum (Invitrogen, UK), 2 mM L-glutamine (Invitrogen, Netherlands), and other components as specified by the suppliers. All cell lines were maintained at 37 $^\circ\text{C}$, 5% CO_2 , and routinely passaged. Short-term growth inhibition was measured using the SRB assay as described previously.^[46] Briefly, cells were seeded at appropriate densities into the wells of 96-well plates in their corresponding medium and incubated overnight to allow the cells to attach. Cells were then exposed to various concentrations of freshly made solutions of drugs and incubated for 96 h. The cells were subsequently fixed with ice-cold trichloroacetic acid (TCA; 10%, w/v) for 30 min and stained with 0.4% SRB dissolved in 1% acetic acid for 15 min. All incubations were carried out at room temperature except for TCA fixation, which was at 4 $^\circ\text{C}$. The IC_{50} value, the concentration required to inhibit cell growth by 50%, was determined from the mean absorbance at 540 nm for each drug concentration expressed as a percentage of the well absorbance in the untreated control.

Computational methods

Molecular model generation: The average structure of the ensemble of unimolecular antiparallel basket-type NMR solution structures of HT G4 (PDB ID: 143D) was chosen as the starting model for the molecular modeling simulations. To ensure that the model was optimally analogous to the human telomeric sequence (F21T) used in the in vitro assays, the 3'-dA nucleotide was removed, two K^+ ions were manually placed in the central cavity, and the final structure was optimized by MD simulation, as previously described.^[21] The indolo[3,2-*c*]quinoline ligand was constructed in the Molecular Operating Environment (MOE) package (www.chemcomp.com) and optimized by density functional theory (DFT) with B3LYP parameterization of the density functional and the 6-31 + G(d,p) basis set, using the Gaussian 03 software package.^[47] Restrained electrostatic potential (RESP) charge derivation of the ligand was obtained from the R.E.D. server, and the ligand topology was obtained from the Automated Topology Builder (ATB), version 2.0.^[48] Partial charges used in MD simulations were obtained

by substituting the charges assigned by the ATB topology with the RESP charges.^[48a] The remaining parameters for the ligand and DNA were obtained from the generalized AMBER03 force field.^[49]

Molecular docking: The MD-optimized G4 structure was prepared with the MOE ver. 2013.08 software package^[39] by removing water molecules and adding the missing hydrogen atoms and protonation states at 300 K, pH 7, with a salt concentration of 0.1 M using the GB/VI electrostatic formalism. The first docking run of the ligand with the G4 structure was performed with the rigid docking protocol included in MOE, using all the G-quadruplex structure as the docking site. The ligand placement obeys the triangle matcher method and the alpha HB free-energy scoring function, retaining the best 100 poses. Final poses were subjected to a final refinement in the receptor pocket with the AMBER99 force field, at an RMS gradient threshold of 0.01 and rescoring with an alpha HB free-energy scoring function. The best-scoring values were selected as final poses for the one ligand per G4 unit model. A second molecular docking run was performed using the final structure of the first MD simulation, already containing one ligand per G4 unit in order to obtain a model of two ligands per G4 unit, using the docking procedure described above.

Molecular dynamics simulations: The models of the antiparallel G4 containing the docked ligands were subjected to MD simulations using the GROMACS simulation package 4.5.5 and applying the AMBER03 force field.^[49] The G4–ligand structures were inserted in a cubic box, with at least 10 Å between the G4 and the simulation box edge. The system was solvated and neutralized by adding the required K⁺ ions. After energy minimization of the MD box with the steepest descent method, a 100 ps NVT equilibration run followed at 298 K (spatially restraining all oligonucleotide atoms) was performed. The final stage equilibration involved a 1 ns run and sampling the NPT ensemble ($T=298$ K, $P=1$ bar) and, finally unconstrained simulation of the system was performed for 50 ns in the same isothermic–isobaric ensemble. In all MD runs, the particle-mesh-Ewald (PME) formalism was applied to the long-range electrostatic interactions. The short-range electrostatic cutoff was 12 Å, and the same length was applied for the van der Waals (vdW) interactions. All bonds were constrained with the Lincs algorithm. Nosé–Hoover and Parrinello–Rahman constraints were applied to control the temperature and isotropic pressure ($\tau_T=0.2$, $\tau_P=5.0$ ps, and $\beta=4.5\times 10^{-5}$ bar⁻¹). Energy and pressure corrections for the vdW cutoff were also applied. Visualizations and images were obtained in MOE ver. 2013.08 and/or with VMD (Visual Molecular Dynamics) software ver. 1.9.^[50]

Free energy calculations: The total free energy of binding and its components for the G4–indolo[3,2-c]quinoline complexes were calculated by the MM-PBSA methodology.^[51] For each system a single trajectory approach was used and the calculations were performed over the last 30 ns of each trajectory. In the MM-PBSA approach an interaction free energy is defined as:

$$\Delta G_{\text{binding}} = G_{\text{complex}} - G_{\text{G4}} - G_{\text{ligand}} \quad (5)$$

$$G = E_{\text{MM}} + G_{\text{polar,sol}} + G_{\text{nonpolar,sol}} - TS \quad (6)$$

$$E_{\text{MM}} = E_{\text{int}} + E_{\text{elec}} + E_{\text{vdW}} \quad (7)$$

The molecular mechanics energy (E_{MM}) includes the contribution of the electrostatic (E_{elec}), van der Waals (E_{vdW}) and internal (E_{int}) energies. E_{elec} was obtained using APBS software package,^[52] as well as the electrostatic contribution to the solvation energy ($G_{\text{polar,sol}}$), and E_{vdW} was calculated by the GROMACS software package.^[49a] The E_{int}

value is cancelled out in [Eq. (7)] due to the single trajectory approach.^[53] The APBS software package was used with a grid spacing of 0.5 Å and an ionic concentration of 100 mM KCl. The interior dielectric constant was set to 1, while the dielectric constant of water was set at 78.4. The atomic charges used in the APBS calculation were taken from the GROMACS force field through the PDB2PQR software.^[54] The nonpolar contribution to the solvation energy, which accounts for the burial of solvent-accessible surface area (SASA) upon binding, was obtained according to $G_{\text{nonpolar,sol}} = \gamma \times \text{SASA} \times \beta$. SASA was obtained in GROMACS, and the γ and β values were set to 2.2 kJ mol⁻¹ nm⁻² and 3.8 kJ mol⁻¹, respectively.^[55] The entropic contribution to the system (TS) is the product of the temperature (298 K) and solute entropy, calculated by GROMACS, is based on the last 20 ns of the 50 ns MD trajectory.

Acknowledgements

The authors thank the Fundação para a Ciência e Tecnologia (FCT, Portugal) for financial support through project grants PEst-OE/SAU/UI4013/2014 and EXPL/QEQ-MED/0502/2012. J.L. also acknowledges the FCT for postdoctoral grant SFRH/BPD/72903/2010, and I.C. acknowledges the FCT for an Investigador FCT position. Work in the Neidle research group (University College London) was supported by the Pancreatic Cancer Research Fund (UK) and the Medical Research Council (UK).

Keywords: antitumor agents · cancer · G-quadruplexes · indolo[3,2-c]quinolones · molecular dynamics

- [1] J. T. Davis, *Angew. Chem. Int. Ed.* **2004**, *43*, 668–698; *Angew. Chem.* **2004**, *116*, 684–716.
- [2] J. Bidzinska, G. Cimino-Reale, N. Zaffaroni, M. Folini, *Molecules* **2013**, *18*, 12368–12395.
- [3] Y. Wu, R. M. Brosh, Jr., *FEBS J.* **2010**, *277*, 3470–3488.
- [4] S. Amrane, A. Kerkour, A. Bedrat, B. Vialet, M. L. Andreola, J. L. Mergny, *J. Am. Chem. Soc.* **2014**, *136*, 5249–5252.
- [5] H. Paritala, S. M. Firestine, *Nucleosides Nucleotides Nucleic Acids* **2010**, *29*, 81–90.
- [6] G. Biffi, D. Tannahill, J. McCafferty, S. Balasubramanian, *Nat. Chem.* **2013**, *5*, 182–186.
- [7] a) A. K. Todd, M. Johnston, S. Neidle, *Nucleic Acids Res.* **2005**, *33*, 2901–2907; b) R. Z. Cer, D. E. Donohue, U. S. Mudunuri, N. A. Temiz, M. A. Loss, N. J. Starner, G. N. Halusa, N. Volfovsky, M. Yi, B. T. Luke, A. Bacolla, J. R. Collins, R. M. Stephens, *Nucleic Acids Res.* **2013**, *41*, D94–D100.
- [8] a) J. L. Huppert, S. Balasubramanian, *Nucleic Acids Res.* **2005**, *33*, 2908–2916; b) S. Balasubramanian, L. H. Hurley, S. Neidle, *Nat. Rev. Drug Discovery* **2011**, *10*, 261–275.
- [9] R. K. Moyzis, J. M. Buckingham, L. S. Cram, M. Dani, L. L. Deaven, M. D. Jones, J. Meyne, R. L. Ratliff, J. R. Wu, *Proc. Natl. Acad. Sci. USA* **1988**, *85*, 6622–6626.
- [10] E. H. Blackburn, *Nature* **1991**, *350*, 569–573.
- [11] a) V. Sekaran, J. Soares, M. B. Jarstfer, *J. Med. Chem.* **2014**, *57*, 521–538; b) N. W. Kim, M. A. Piatyszek, K. R. Prowse, C. B. Harley, M. D. West, P. L. C. Ho, G. M. Coviello, W. E. Wright, S. L. Weinrich, J. W. Shay, *Science* **1994**, *266*, 2011–2015; c) A. M. Zahler, J. R. Williamson, T. R. Cech, D. M. Prescott, *Nature* **1991**, *350*, 718–720; d) B. Maji, S. Bhattacharya, *Chem. Commun.* **2014**, *50*, 6422–6438.
- [12] a) M. L. Bochman, K. Paeschke, V. A. Zakian, *Nat. Rev. Genet.* **2012**, *13*, 770–780; b) S. A. Ohnmacht, M. Micco, V. Petrucci, A. K. Todd, A. P. Reszka, M. Gunaratnam, M. A. Carvalho, M. Zloh, S. Neidle, *Bioorg. Med. Chem. Lett.* **2012**, *22*, 5930–5935.
- [13] a) C. Douarre, X. Mergui, A. Sidibe, D. Gomez, P. Alberti, P. Mailliet, C. Trentesaux, J. F. Riou, *Nucleic Acids Res.* **2013**, *41*, 3588–3599; b) P. Murat, S. Balasubramanian, *Curr. Opin. Genet. Dev.* **2014**, *25*, 22–29.

- [14] M. Döchler, *J. Drug Targeting* **2012**, *20*, 389–400.
- [15] a) S. A. Ohnmacht, S. Neidle, *Bioorg. Med. Chem. Lett.* **2014**, *24*, 2602–2612; b) S. Zhang, Y. Wu, W. Zhang, *ChemMedChem* **2014**, *9*, 899–911; c) Y. Yan, J. Tan, T. Ou, Z. Huang, L. Gu, *Expert Opin. Ther. Pat.* **2013**, *23*, 1495–1509.
- [16] P. Murat, Y. Singh, E. Defranco, *Chem. Soc. Rev.* **2011**, *40*, 5293–5307.
- [17] a) W. Xu, J. H. Tan, S. B. Chen, J. Q. Hou, D. Li, Z. S. Huang, L. Q. Gu, *Biochem. Biophys. Res. Commun.* **2011**, *406*, 454–458; b) J. Lavrado, R. Moreira, A. Paulo, *Curr. Med. Chem.* **2010**, *17*, 2348–2370; c) T. M. Ou, J. Lin, Y. J. Lu, J. Q. Hou, J. H. Tan, S. H. Chen, Z. Li, Y. P. Li, D. Li, L. Q. Gu, Z. S. Huang, *J. Med. Chem.* **2011**, *54*, 5671–5679; d) F. Riechert-Krause, K. Weisz, *Heterocycl. Commun.* **2013**, *19*, 145–166.
- [18] B. Guyen, C. M. Schultes, P. Hazel, J. Mann, S. Neidle, *Org. Biomol. Chem.* **2004**, *2*, 981–988.
- [19] Y. X. Xiong, Z. S. Huang, J. H. Tan, *Eur. J. Med. Chem.* **2015**, DOI: 10.1016/j.ejmech.2014.11.021.
- [20] J. Lavrado, A. P. Reszka, R. Moreira, S. Neidle, A. Paulo, *Bioorg. Med. Chem. Lett.* **2010**, *20*, 7042–7045.
- [21] J. Lavrado, P. M. Borralho, S. A. Ohnmacht, R. E. Castro, C. M. Rodrigues, R. Moreira, D. J. V. A. dos Santos, S. Neidle, A. Paulo, *ChemMedChem* **2013**, *8*, 1648–1661.
- [22] R. G. Gould, W. A. Jacobs, *J. Am. Chem. Soc.* **1939**, *61*, 2890–2895.
- [23] A. Molina, J. J. Vaquero, J. L. GarciaNavio, J. AlvarezBuilla, B. dePascual-Teresa, F. Gago, M. M. Rodrigo, M. Ballesteros, *J. Org. Chem.* **1996**, *61*, 5587–5599.
- [24] C. M. P. Pereira, H. A. Stefani, K. P. Guzen, A. T. G. Orfao, *Lett. Org. Chem.* **2007**, *4*, 43–46.
- [25] P. V. Boddupally, S. Hahn, C. Beman, B. De, T. A. Brooks, V. Gokhale, L. H. Hurley, *J. Med. Chem.* **2012**, *55*, 6076–6086.
- [26] Y. J. Lu, T. M. Ou, J. H. Tan, J. Q. Hou, W. Y. Shao, D. Peng, N. Sun, X. D. Wang, W. B. Wu, X. Z. Bu, Z. S. Huang, D. L. Ma, K. Y. Wong, L. Q. Gu, *J. Med. Chem.* **2008**, *51*, 6381–6392.
- [27] a) S. Gogoi, A. E. Shchekotikhin, A. Membrino, Y. B. Sinkevich, L. E. Xodo, *J. Med. Chem.* **2013**, *56*, 2764–2778; b) F. Cuenca, M. J. Moore, K. Johnson, B. Guyen, A. De Cian, S. Neidle, *Bioorg. Med. Chem. Lett.* **2009**, *19*, 5109–5113.
- [28] F. W. Dahlquist, *Methods Enzymol.* **1978**, *48*, 270–299.
- [29] J. D. McGhee, P. H. von Hippel, *J. Mol. Biol.* **1974**, *86*, 469–489.
- [30] A. Arora, C. Balasubramanian, N. Kumar, S. Agrawal, R. P. Ojha, S. Maiti, *FEBS J.* **2008**, *275*, 3971–3983.
- [31] C. Wei, L. Wang, G. Jia, J. Zhou, G. Han, C. Li, *Biophys. Chem.* **2009**, *143*, 79–84.
- [32] a) J. X. Pan, S. P. Zhang, *J. Biol. Inorg. Chem.* **2009**, *14*, 401–407; b) L. Martino, A. Virno, B. Pagano, A. Virgilio, S. Di Micco, A. Galeone, C. Giancola, G. Bifulco, L. Mayol, A. Randazzo, *J. Am. Chem. Soc.* **2007**, *129*, 16048–16056.
- [33] C. Y. Huang, *Methods Enzymol.* **1982**, *87*, 509–525.
- [34] J. Dai, M. Carver, D. Yang, *Biochimie* **2008**, *90*, 1172–1183.
- [35] A. I. Karsisiotis, N. M. Hessari, E. Novellino, G. P. Spada, A. Randazzo, M. W. da Silva, *Angew. Chem. Int. Ed.* **2011**, *50*, 10645–10648; *Angew. Chem.* **2011**, *123*, 10833–10836.
- [36] S. Ghosh, S. K. Pradhan, A. Kar, S. Chowdhury, D. Dasgupta, *Biochim. Biophys. Acta* **2013**, *1830*, 4189–4201.
- [37] L. Martino, B. Pagano, I. Fotticchia, S. Neidle, C. Giancola, *J. Phys. Chem. B* **2009**, *113*, 14779–14786.
- [38] Y. Wang, D. J. Patel, *Structure* **1993**, *1*, 263–282.
- [39] Molecular Operating Environment (MOE) ver. 2013.08, Chemical Computing Group Inc., Montreal, QC (Canada), **2013**.
- [40] N. H. Campbell, M. Patel, A. B. Tofa, R. Ghosh, G. N. Parkinson, S. Neidle, *Biochemistry* **2009**, *48*, 1675–1680.
- [41] P. A. Kollman, I. Massova, C. Reyes, B. Kuhn, S. H. Huo, L. Chong, M. Lee, T. Lee, Y. Duan, W. Wang, O. Donini, P. Cieplak, J. Srinivasan, D. A. Case, T. E. Cheatham, *Acc. Chem. Res.* **2000**, *33*, 889–897.
- [42] A. M. Ferrari, G. Degliesposti, M. Sgobba, G. Rastelli, *Bioorg. Med. Chem.* **2007**, *15*, 7865–7877.
- [43] S. Mpima, S. A. Ohnmacht, M. Barletta, J. Husby, L. C. Pett, M. Gunaratnam, S. T. Hilton, S. Neidle, *Bioorg. Med. Chem.* **2013**, *21*, 6162–6170.
- [44] F. S. Di Leva, E. Novellino, A. Cavalli, M. Parrinello, V. Limongelli, *Nucleic Acids Res.* **2014**, *42*, 5447–5455.
- [45] M. Micco, G. W. Collie, A. G. Dale, S. A. Ohnmacht, I. Pazitna, M. Gunaratnam, A. P. Reszka, S. Neidle, *J. Med. Chem.* **2013**, *56*, 2959–2974.
- [46] V. Vichai, K. Kirtikara, *Nat. Protoc.* **2006**, *1*, 1112–1116.
- [47] Gaussian 03, Revision C2. M. J. Frisch, G. W. Trucks, H. B. Schlegel, G. E. Scuseria, M. A. Robb, J. R. Cheeseman, J. A. Montgomery, Jr., T. Vreven, K. N. Kudin, J. C. Burant, J. M. Millam, S. S. Iyengar, J. B. Tomasi, V. B. Mennucci, M. S. Cossi, G., N. Rega, G. A. Petersson, H. Nakatsuji, M. Hada, M. Ehara, K. Toyota, R. Fukuda, J. Hasegawa, M. Ishida, T. Nakajima, Y. Honda, O. Kitao, H. Nakai, M. Klene, X. Li, J. E. Knox, H. P. Hratchian, J. B. Cross, C. Adamo, J. Jaramillo, R. Gomperts, R. E. Stratmann, O. Yazyev, A. J. Austin, R. Cammi, C. Pomelli, J. W. Ochterski, P. Y. Ayala, K. Morokuma, G. A. Voth, P. Salvador, J. J. Dannenberg, V. G. Zakrzewski, S. Dapprich, A. D. Daniels, M. C. Strain, O. Farkas, D. K. Malick, A. D. Rabuck, K. Raghavachari, J. B. Foresman, J. V. Ortiz, Q. Cui, A. G. Baboul, S. Clifford, J. Cioslowski, B. B. Stefanov, G. Liu, A. Liashenko, P. Piskorz, I. Komaromi, R. L. Martin, D. J. Fox, T. Keith, M. A. Al-Laham, C. Y. Peng, A. Nanayakkara, M. Challacombe, P. M. W. Gill, B. Johnson, W. Chen, M. W. Wong, C. Gonzalez, J. A. Pople, Gaussian Inc., Wallingford, CT, **2004**.
- [48] a) E. Vanqualef, S. Simon, G. Marquant, E. Garcia, G. Klimerak, J. C. Delepine, P. Cieplak, F. Y. Dupradeau, *Nucleic Acids Res.* **2011**, *39*, W511–W517; b) A. K. Malde, L. Zuo, M. Breeze, M. Stroet, D. Poger, P. C. Nair, C. Oostenbrink, A. E. Mark, *J. Chem. Theory Comput.* **2011**, *7*, 4026–4037.
- [49] a) D. Van der Spoel, E. Lindahl, B. Hess, G. Groenhof, A. E. Mark, H. J. C. Berendsen, *J. Comput. Chem.* **2005**, *26*, 1701–1718; b) L. J. Yang, C. H. Tan, M. J. Hsieh, J. M. Wang, Y. Duan, P. Cieplak, J. Caldwell, P. A. Kollman, R. Luo, *J. Phys. Chem. B* **2006**, *110*, 13166–13176.
- [50] W. Humphrey, A. Dalke, K. Schulten, *J. Mol. Graphics Modell.* **1996**, *14*, 33–38.
- [51] J. M. J. Swanson, R. H. Henchman, J. A. McCammon, *Biophys. J.* **2004**, *86*, 67–74.
- [52] N. A. Baker, D. Sept, S. Joseph, M. J. Holst, J. A. McCammon, *Proc. Natl. Acad. Sci. USA* **2001**, *98*, 10037–10041.
- [53] R. E. Amaro, X. L. Cheng, I. Ivanov, D. Xu, J. A. McCammon, *J. Am. Chem. Soc.* **2009**, *131*, 4702–4709.
- [54] T. J. Dolinsky, P. Czodrowski, H. Li, J. E. Nielsen, J. H. Jensen, G. Klebe, N. A. Baker, *Nucleic Acids Res.* **2007**, *35*, W522–W525.
- [55] W. Wang, P. A. Kollman, *Proc. Natl. Acad. Sci. USA* **2001**, *98*, 14937–14942.

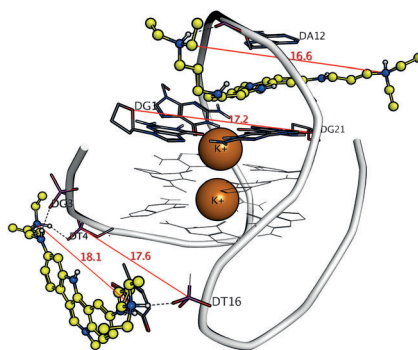
Received: February 11, 2015

Revised: March 4, 2015

Published online on ■■■■■, 0000

FULL PAPERS

A much higher IQ: We report indolo[3,2-*c*]quinoline (IQc) derivatives with two weak basic side chains as potent and selective human telomeric (HT) G-quadruplex (G4) stabilizers. Biophysical data show that stabilization involves the binding of two ligands which induces a conformational rearrangement of the HT G4 structure. Moreover, selected derivatives showed selective antiproliferative activity toward human malignant cell lines.



J. Lavrado, S. A. Ohnmacht, I. Correia, C. Leitão, S. Pisco, M. Gunaratnam, R. Moreira, S. Neidle, D. J. V. A. d. Santos, A. Paulo*



Indolo[3,2-*c*]quinoline G-Quadruplex Stabilizers: a Structural Analysis of Binding to the Human Telomeric G-Quadruplex

